Micro- to nanoscale textures of gold in arsenopyrite and scorodite from the As-Au-Bi assemblage of Drenjak locality (Serbia)

Ivana Jelić, Janez Zavašnik, Marina Lazarov, Alena Zdravković, Sabina Kovač, Jovica Stojanović, Aleksandar Pačevski

Micro- to nanoscale textures of gold in arsenopyrite and scorodite from the As-Au-Bi assemblage of Drenjak locality (Serbia) | Ivana Jelić, Janez Zavašnik, Marina Lazarov, Alena Zdravković, Sabina Kovač, Jovica Stojanović, Aleksandar Pačevski | Ore Geology Reviews | 2023 | |

10.1016/j.oregeorev.2023.105711

http://dr.rgf.bg.ac.rs/s/repo/item/0008409

Ore Geology Reviews 163 (2023) 105711

Contents lists available at ScienceDirect

Ore Geology Reviews

journal homepage: www.elsevier.com/locate/oregeorev

Micro- to nanoscale textures of gold in arsenopyrite and scorodite from the As-Au-Bi assemblage of Drenjak locality (Serbia)

Ivana Jelić [a], Janez Zavašnik [b,*], Marina Lazarov [c], Alena Zdravković [a], Sabina Kovač [a], Jovica Stojanović [d], Aleksandar Pačevski [a,*]

[a] University of Belgrade – Faculty of Mining and Geology, Đušina 7, 11000 Belgrade, Serbia
[b] Jožef Stefan Institute, Jamova cesta 39, Ljubljana 1000, Slovenia
[c] Institute für Mineralogie, Leibniz Universität Hannover, Callinstr. 3, 30167 Hannover, Germany
[d] Applied Mineralogy Unit, Institute for Technology of Nuclear and Other Mineral Raw Materials, Franchet d'Esperey 86, 11000 Belgrade, Serbia

ARTICLE INFO

Keywords:
Arsenopyrite
Scorodite
Gold
Native bismuth
Bi-arsenate
Gold nanocrystallites

ABSTRACT

Arsenopyrite and pyrite are important carriers of Au that is present in the form of microscopic and "invisible" gold. Such gold can be expected to be released upon the process of oxidation of these sulfides. In studied gold mineralization at Drenjak, related to the granitoids of the Oligocene-Miocene Kopaonik Ore District, the main arsenopyrite-pyrite-(bismuthinite) sulfide assemblage was formed in the quartz bodies and partly replaced by scorodite ($FeAsO_4{\cdot}2H_2O$) and Bi-arsenate. With only up to 5 ppm of gold recorded by LA-ICP-MS, aforementioned sulfide minerals are here practically free from lattice-bound gold. Native gold is present in the mineralization, generally ranging in grain size from 20 μm down to the nanoparticles, as revealed by TEM. It is mainly hosted by arsenopyrite and scorodite. In arsenopyrite, gold is polycrystalline and consists of nanocrystallites 20–30 nm in size. It was deposited after arsenopyrite, healing its cavities and microcracks, often associated with native bismuth and bismuthinite. The abundance of gold and Bi minerals correlates with the presence of scorodite. Two types of gold are present in scorodite and Bi arsenate: i) prevailing relict Au grains retained after arsenopyrite oxidation, ii) colloidal-like gold co-precipitated with the arsenates. Based on our observations, we additionally present and discuss indications of low-temperature hydrothermal origin of scorodite, formerly known only as a weathering product

1. Introduction

Gold-bearing arsenopyrite and As-Au correlation is a well-known phenomenon in nature that is present in numerous types of ore deposits. Despite the intensive research in this area driven by the economic value of gold (e.g. references below), the fundamental cause of the Au-As relationship yet remain unresolved (Pokrovski et al., 2002, 2021). Gold in arsenopyrite and arsenian pyrite usually occurs either in the form of μm-sized grains or, in the form of "invisible gold" referring to both submicroscopic (i.e. nm-sized gold) as well as structurally bound gold (Cabri et al., 1989, 2000, Fleet and Mumin, 1997, Genkin et al., 1998, Pokrovski et al., 2021). Regarding the accumulation processes of Au, the theories are even more diverse: some studies suggest that the accumulation of gold in arsenopyrite is controlled by the electrochemical processes (Möller et al., 1997), by the rate of oxidation of arsenopyrite (Madox et al., 1998) and coupled Au-As redox reactions (Pokrovski et al., 2021). On the other hand, nm- to μm-scale gold grains can be formed by the remobilization of Au from arsenopyrite structure caused by subsequent deformation events, such as those typical for orogenic lode-gold systems (Sung et al., 2009, Cook et al., 2013). In addition to the As-Au correlation, the Au-Bi system is also commonly found in nature. Bismuth is often a scavenger of gold in hydrothermal solutions, and a great number of examples from various types of deposits were summarized in the recent review paper of Deady et al. (2022). Furthermore, a triple-mix of As-Au-Bi assemblages is also not rare in nature (e.g. Acosta-Góngora et al., 2015, Jonasson, 2018, Meng et al., 2022).

During an oxidation process, both μm-sized and "invisible gold" are released from the host sulfide and subjected to migration, transport and accumulation. Scorodite is one of the main oxidation products of arsenopyrite, interpreted as a secondary mineral originating in weathering processes; the hydrothermal origin is not reported in the literature. It is

* Corresponding authors.
E-mail addresses: janez.zavasnik@ijs.si (J. Zavašnik), aleksandar.pacevski@rgf.bg.ac.rs (A. Pačevski).

https://doi.org/10.1016/j.oregeorev.2023.105711
Received 25 November 2022; Received in revised form 30 May 2023; Accepted 5 October 2023
Available online 3 November 2023

widely researched as a secondary phase of mine tailing environments (e.g. Roussel et al., 2000, Walker et al., 2009, Murciego et al., 2011), mainly because it is the most suitable phase for arsenic storage in the environments due to its non-toxicity and stability under a wide range of surface conditions (e.g. Harvey et al., 2006, Majzlan et al., 2012, Shibata et al., 2012). On the other side, since arsenopyrite is a sulfide mineral that concentrates gold to the greatest extent (Cook and Chryssoulis, 1990), enrichment of this precious metal can also be expected in scorodite. However, the presence of gold in scorodite associated with Au-bearing arsenopyrite is only sporadically mentioned in some studies (Akiska et al., 2008, Cherepanova, 2009, Boboev and Tabarov, 2021, Ishbobaev et al., 2021). There is no extensive research on this topic, especially regarding the grain size and morphology of gold within this mineral.

In this study, we present a mode of gold occurrence in arsenopyrite and scorodite based on the textures documented in the micro- to nanoscale range and discuss possibility for the hydrothermal origin of scorodite in nature.

2. Geological setting and sampling

The Drenjak locality is situated in the Gokčanica area on the western slope of Željin mountain, a part of the Kopaonik Ore District (KOD). This ore district belongs to the Serbomacedonian-Rhodope Metallogenetic Belt (SRMB) of the Oligocene-Miocene age (Fig. 1a,b). The SRMB is related to calc-alkaline magmatism showing evidence chiefly for continent–continent collision and only sporadically for a direct relation to subduction, mainly in the south-eastern (SE) sector (Heinrich and Neubauer, 2002, Cvetković et al., 2013 and references therein). Two types of deposits predominate in the SRMB; 1) meso- to epithermal Pb-Zn-(±Sb,Ag,Au) vein and carbonate replacement deposits generally extending in the north-western sector to which KOD belongs and, 2) porphyry Cu-Mo-Au and epithermal Au deposits which are more common in SE sector (Janković, 1997, Heinrich and Neubauer, 2002).

The KOD is characterized by the striking structural feature of the Željin–Kopaonik anticlinorium with N–S axis sinking to the North (Urosević et al., 1973a,b, Lesić et al., 2013, 2019). The oldest rocks forming the anticlinorium are Late Palaeozoic to Early Jurassic metamorphosed sediments mainly presented by the schists (Urosević et al., 1973a,b), called Kopaonik metamorphic complex (Zelić et al., 2010). It is overlain by the ophiolitic complex of generally Jurassic age. The Kopaonik metamorphic complex is intruded by I-type granitoids of the Oligocene-Miocene age. These granitoids exhibit some variation in mineralogical and chemical composition but are dominantly granodiorites. Accompanying volcanic rocks of dacite-andesite composition are also present and are especially abundant in the southern part of the district. The KOD represents one of the most ore-bearing districts in SRMB and SE Europe in general, including numerous Pb-Zn deposits, among which is the world-famous Trepča deposit (Fig. 1b). Most of these and other types of deposits are located in the southern part of the district and are often related to the volcanics representing part of the magmatic-volcanic system.

On the other side, studied mineralization at Drenjak occurs in the northern part of the district and belongs to the mineralization suite of Gokčanica and Plana areas (Fig. 1b,c). In these areas, as in the entire KOD, there are numerous traces of medieval mining such as slag, pits, and similar, as evidence of intensive mining activity in the past (e.g. Vranić, 2021). In recent time, systematic and comprehensive geological explorations of Gokčanica and Plana were carried out in the mid-twentieth century. On that occasion, some of old adits were restored and new ones were opened, and the research data were published in the papers Maksimović and Divljan (1953) and Deleon (1954). It was found that sulfide mineralizations have been pretty widespread, but mainly represented by pyrite and arsenopyrite, with minor to insignificant participation of Cu, Pb, Zn, Au, Ag, Bi, Ni, Co minerals. For this reason, no further comprehensive geological investigations were carried out, but only sporadic ones, which in the area of Gokčanica have focused mainly on the occurrence of gold in Drenjak, the subject also of the present study.

Sulfide mineralization in Gokčanica and Plana is associated with outcrops of diorite, quartz diorite, microdiorite and andesite, intruded in serpentinite that is often altered to carbonate–silicate rocks near to the contacts (Fig. 1c). The outcrops are genetically related to the Željin granitoid, and Maksimović and Divljan (1953) classified them in two arrays with a NNW-SSE direction: the first one (Kosovci-Lajštak-Rastova glava) is closer to the Željin intrusive and without noticeable mineralizations, and the second group (Rudnjak-Drenjak-Plana direction) in which the hydrothermal activities and mineralization processes were developed. The hydrothermal phase left no traces only in the diorite of Dubovo; the researchers considered that it was transferred to the neighbouring microdiorites. They further concluded that diorites and microdiorites had been intruded during the time interval between the formation of Željin granitoide and andesitic volcanism. According to their observations, mineralizations related to microdiorites are characterized by the presence of Bi minerals. While, those related to andesites to a greater extent contain Pb-Zn, especially in the Plana area. The formation of significant Pb-Zn deposits (Sastavci, Kiževak, etc.) begins with volcanic activities south of Plana, which have a more pronounced dacite-andesite character.

The outcrops of mineralized microdiorite occur in the localities of Drenjak, Rujak and, to a lesser extent, Rudnjak. This rock is holocrystalline, and generally consists of plagioclase highly altered to sericite, and hornblende that is almost completely transformed into chlorite, while biotite, and also secondary albite and calcite are sporadically to rarely present (Maksimović and Divljan, 1953). Sulfide mineralization, generally consisting of arsenopyrite and pyrite, occurs in the quartz veins and irregular bodies mainly within microdiorite and to a lesser extent along its contact with the hydrothermally altered serpentinite.

At Drenjak, mineralized quartz veins and bodies up to several meters in size are oriented in the ENE-WSW direction. This mineralization was explored by two adits opened in 1951 in lengths of 67 and 93 m, respectively (Fig. 1d). In some sections of the adits, the microdiorite was intensively crushed, limonized and kaolinized. Subsequent movement and brecciation were also observed in the quartz bodies, where arsenopyrite and pyrite were intensively cataclized (Maksimović and Divljan, 1953). Deleon (1954) gave a detailed description of the mineralization and stated that arsenopyrite comprised about 90 % of the sulfides, the rest being mainly pyrite. He further mentioned the sporadic occurrence of chalcopyrite, sphalerite and pyrrhotite, and pointed out the noticeable occurrence of bismuthinite up to 2 mm in size and native bismuth up to 0.1 mm. Finally, he often noted the presence of scorodite crusts after arsenopyrite.

At Rujak, the mineralization of a similar type was explored with a 36 m long adit that intersected several sulfide-bearing quartz veins up to 0.5 mm thick. The veins were localized in intensively propylitized microdiorite and at its contact with the hydrothermally altered serpentinite (Maksimović and Divljan, 1953). Deleon (1954) stated that the mineralization at Rujak is quite similar to that at Drenjak, and noted some variations between them. Namely, the mineralization at Rujak showed a more significant presence of pyrrhotite, which was deposited after arsenopyrite, then, lesser abundance of arsenopyrite, and an absence of native bismuth. Due to the absence of native bismuth, he suggested that the mineralization at Rujak was formed from a high- to medium-temperature hydrothermal stage, while at Drenjak, the deposition continued at lower temperatures. He further assumed that, related to that depositional difference, the gold content is higher in Drenjak (Rujak – 6 ppm Au, Drenjak – 15 ppm Au; the author did not specify what probes these contents refer to).

Later, Popović (1992) found elevated gold content at Drenjak of up to 80 ppm in some probes of this mineralization. However, this author, like Deleon (1954), did not determine a mode of gold occurrence in the

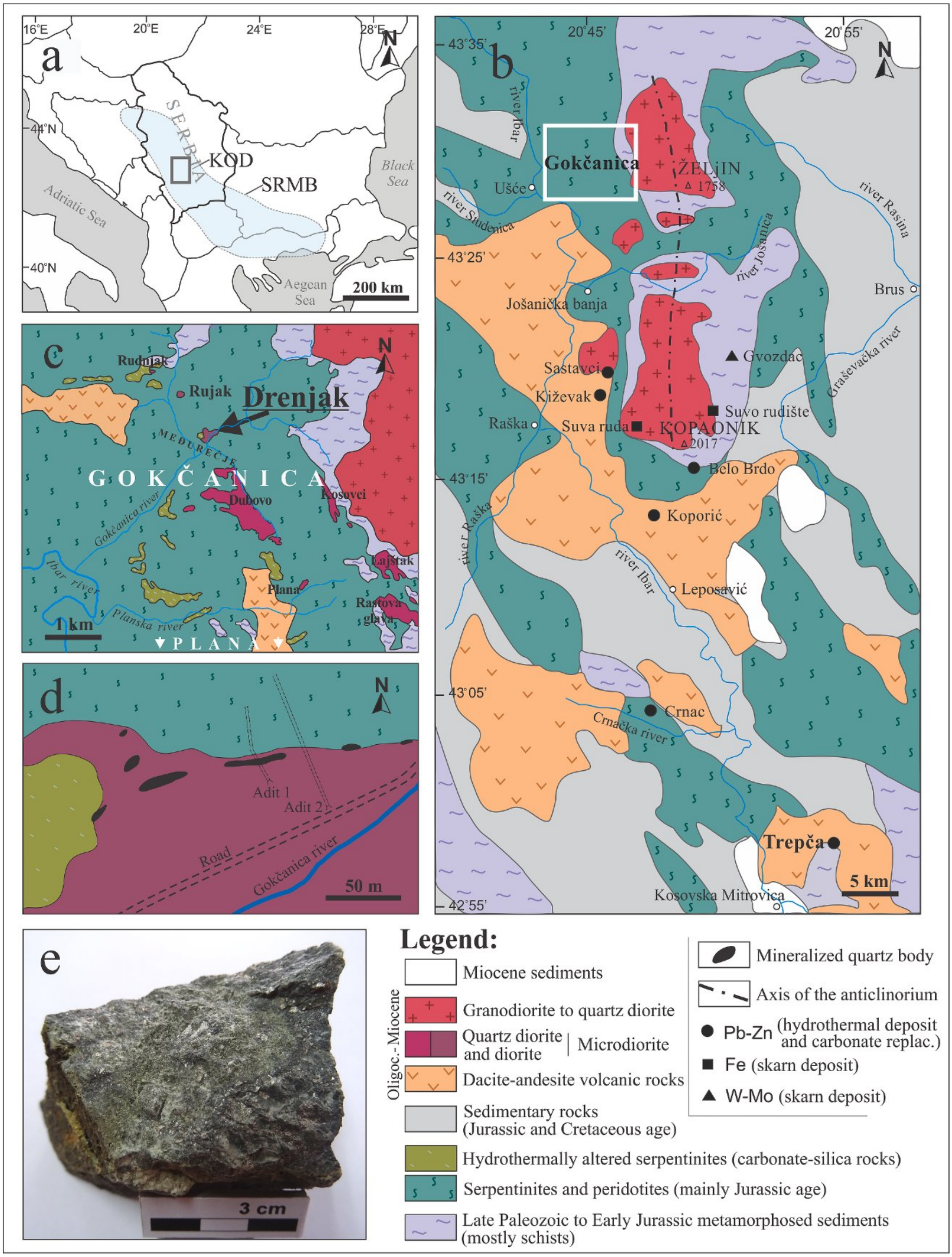

Fig. 1. A. Geographic position of the Kopaonik Ore District (KOD), part of the Serbomacedonian-Rhodope Metallogenetic Belt (SRMB). b. Geological map of the KOD (after Urosević et al., 1973a,b, simplified) with the position of the Gokčanica area and the main ore deposits. c. Geological map of the Gokčanica area (after Maksimović and Divljan, 1953). d. Geological sketch of the studied Drenjak locality (after Maksimović and Divljan, 1953). e. A typical sample from the mineralized quartz bodies of Drenjak, showing abundant arsenopyrite (metallic luster) and a greenish tint due to the presence of scorodite.

ore, than Popović (1992) only speculated that it was related to arsenopyrite. The presence of fine grains of native gold in arsenopyrite and scorodite was revealed by Pačevski (2002), indicating the necessity for more detailed investigations of this gold occurrence. Several companies have partially explored this mineralization in recent decades, but no sufficient and suitable gold reserves for exploitation have yet been established.

Studied samples from the Drenjak were collected mainly by the former exploration of several mineralization localities in the Gokčanica area (Pačevski, 2002). During the research 8 samples noted from T1-1 to T1-8 were collected from the mining dump in front adit 1 of Drenjak (Fig. 1e). Four samples in this study, labelled FSC7 to FSC10, are from the earlier explorations of adits 1 and 2 conducted by Maksimović and Divljan (1953) and Deleon (1954) and were preserved within the Faculty Sample Collection (FSC). All samples are visually similar, and no significant difference in mineral composition and ore texture was observed between these two sets of samples.

3. Methods

Polished sections and thin polished sections, prepared from the studied samples, were first conventionally investigated by polarized light microscopy, mostly in reflected light. Microscopic examinations were then continued using JEOL JSM–6610LV scanning electron microscope (SEM) at the University of Belgrade – Faculty of Mining and Geology. This SEM is equipped with an energy-dispersive spectrometer (EDS) of Oxford Instruments, model X-Max Large Area Analytical Silicon Drift Detector, connected with INCAEnergy 350 Microanalysis System. An acceleration voltage of 20 kV was used for the analyses. Before observation, the polished sections were sputtered by a nm-thick carbon layer to prevent charging. One piece of sample T1-2 is sputtered by gold to obtain a high-quality image of the scorodite crystal habit. The composition of the minerals was routinely checked by SEM-EDS, using internal standards of the Oxford Instruments software. Obtained major element compositions were used for the internal standardization of the trace element measurements.

Trace element composition of arsenopyrite, pyrite, tetrahedrite and bismuthinite were determined in situ. Used were femtosecond laser ablation (fs-LA) system (Solstice, Spectra-Physics, USA) coupled to the Element 2 XR (Thermo Scientific, Germany) Inductively Coupled Plasma Mass Spectrometer (ICP-MS) at the Institut für Mineralogie, Leibniz Universität Hannover, Germany. The laser unit operates in the deep UV at 194 nm and produces energy pulses of around 50 mJ in the fourth harmonic (Horn, 2008, Albrecht et al., 2014, Oeser et al., 2014). The He gas carried ablated sample from the laser cell was admixed with the Ar gas prior entering the ICP-MS. The NIST 610 glass reference material was used as an external standard. The laser beam diameter of 60 μm and frequency of 15 Hz was used for standard, while for the sulfides laser spot size of 20–40 μm and frequency of 5–15 Hz were adjusted to the grain size. The "X" - skimmer and the "jet" – sampler cones were used to achieve measurement of low trace element contents. The oxide formation was held as low as 0.4 % of ThO/Th. The NIST 610 glass reference material was used as an external standard. The SEM-EDS obtained major elements, Fe for arsenopyrite and pyrite, Zn for tetrahedrite and S for bismuthinite, were used for the internal standardization. Data reduction and drift correction was performed in the Matlab-based SILLS program (Guillong et al., 2008). The nickel sulfide PGE-A standard was measured several times during the session and calculated as unknown. The reproducibility of the PGE-A was better than 10 % for all measured elements.

One piece of key sample T1-2 was powdered and analyzed by X-ray diffraction (XRD) method using Rigaku SmartLab powder X-ray diffractometer at room temperature and applying Bragg–Brentano geometry and Cu-Kα radiation. The diffractometer was operated at 40 kV and 30 mA, while the scan range was from 2 to 70° 2θ, with a step size of 0.01° 2θ and a scanning speed of 10° 2θ min^{-1}. The phases were identified using Rigaku PDXL 2 software and the PDF-2 database (International Centre for Diffraction Data).

Arsenopyrite from T1-2 was additionally investigated by Transmission Electron Microscope (TEM) at the Jožef Stefan Institute (Slovenia). The electron-transparent samples for TEM analyses were extracted from a polished bulk sample T1-2, pre-analysed by OM and SEM. From the pre-selected Au-rich arsenopyrite region, a θ 2.3 mm core was drilled by the ultrasonic drill (Ultrasonic Cutter 380, Sonicut), mounted by epoxy resin (G2, Gatan) in a θ 3 mm brass tube, and sliced and polished into 100 μm disks. Further, the samples were pre-thinned at the disk centre down to 10 μm (Dimple Grinder Mod. 656, Gatan) and Ar + ion-etched until perforation by precision ion polishing system (PIPS Mod. 691, Gatan) at 4 keV and incident angle of 8°. Such prepared samples were mounted in low-background dual tilt beryllium holder and analyzed in a 200 kV transmission electron microscope (JEM-2100, JEOL), additionally equipped with Energy-dispersive X-ray spectrometer (EDS, EX-24063JGT, JEOL). Micrographs were recorded with slow-scan CCD camera (Orius SC1000, Gatan).

4. Results

4.1. Mineral assemblage and gold occurrence

Arsenopyrite, partly replaced by scorodite, is the predominant sulfide in the quartz bodies at Drenjak, (Fig. 1e), while pyrite is also locally present in larger quantities. We estimate that these two sulfides make up about 99 % of the sulfide phase (arsenopyrite ~ 90 % and pyrite 5–10 %). Of the other sulfides, only bismuthite is slightly more present and occurs in milimeter-sized aggregates. Thus, studied mineralization at Drenjak generally consists of quartz-arsenopyrite-pyrite-bismuthinite-scorodite mineral assemblage (Fig. 2). The content of scorodite varies significantly; in some parts of the mineralization it is entirely absent, while in others it is one of the main constituents (Fig. 3). Scorodite was unequivocally determined by XRD (Fig. 4). Native bismuth, Bi-arsenate, chalcopyrite, tetrahedrite, sphalerite, galena, native gold, pyrrhotite and tetradymite represent rare minerals (listed in decreasing quantities), present only in microscopic-sized grains.

Native gold almost exclusively occurs in fine grains up to 20 μm in size hosted by arsenopyrite and scorodite, often associating with Bi minerals (Fig. 5a-f). Only in one case chalcopyrite is also present within this assemblage (Fig. 5g). Similarly, only one slightly larger gold grain (~40 μm) is found purely in bismuthinite, outside arsenopyrite and scorodite (Fig. 5h). The size of gold grains is often close to and below the resolution limit of polarized light microscopy and SEM methods, going down to the nanoscale level of grain size in both arsenopyrite (Fig. 6a,b) and scorodite (Fig. 6c,d).

Mineralization processes at Drenjak can be divided into three stages of deposition, in which two generations of gold are recognized.

Stage 1 is the main sulfide-bearing hydrothermal stage in which arsenopyrite and pyrite crystallized. These minerals occur as coarse anhedral to subhedral grains up to 5 mm in size and coarse-grained aggregates, which were frequently cataclized and cemented by quartz (Fig. 2a, 3a). Minor amounts of bismuthinite and a quite rare tetradymite are also present in this depositional sequence, mostly forming fine grains (<30 μm) in arsenopyrite. Bismuthinite rarely occurs in slightly larger grains up to 0.2 mm in size closely associating with arsenopyrite.

Stage 2 represents the mineralization process that formed gold enrichment followed by bismuth and quite weak Cu-Pb-Zn mineralization. A major portion of bismuthinite was deposited within this stage. Bismuthinite only locally forms larger grains up to 1–2 mm in size, and it mainly occurs as fine grains up to 0.2 mm, often along the cracks and rims of arsenopyrite (Fig. 2b). Negligible present fine grains of chalcopyrite and tetrahedrite in a few places also fills the microcracks in arsenopyrite (Fig. 5g, 3c, respectively). Quite rare pyrrhotite up to 30 μm in size, associating with bismuthinite, is also found in arsenopyrite cavities. Galena and sphalerite are also rarely present and occur only as

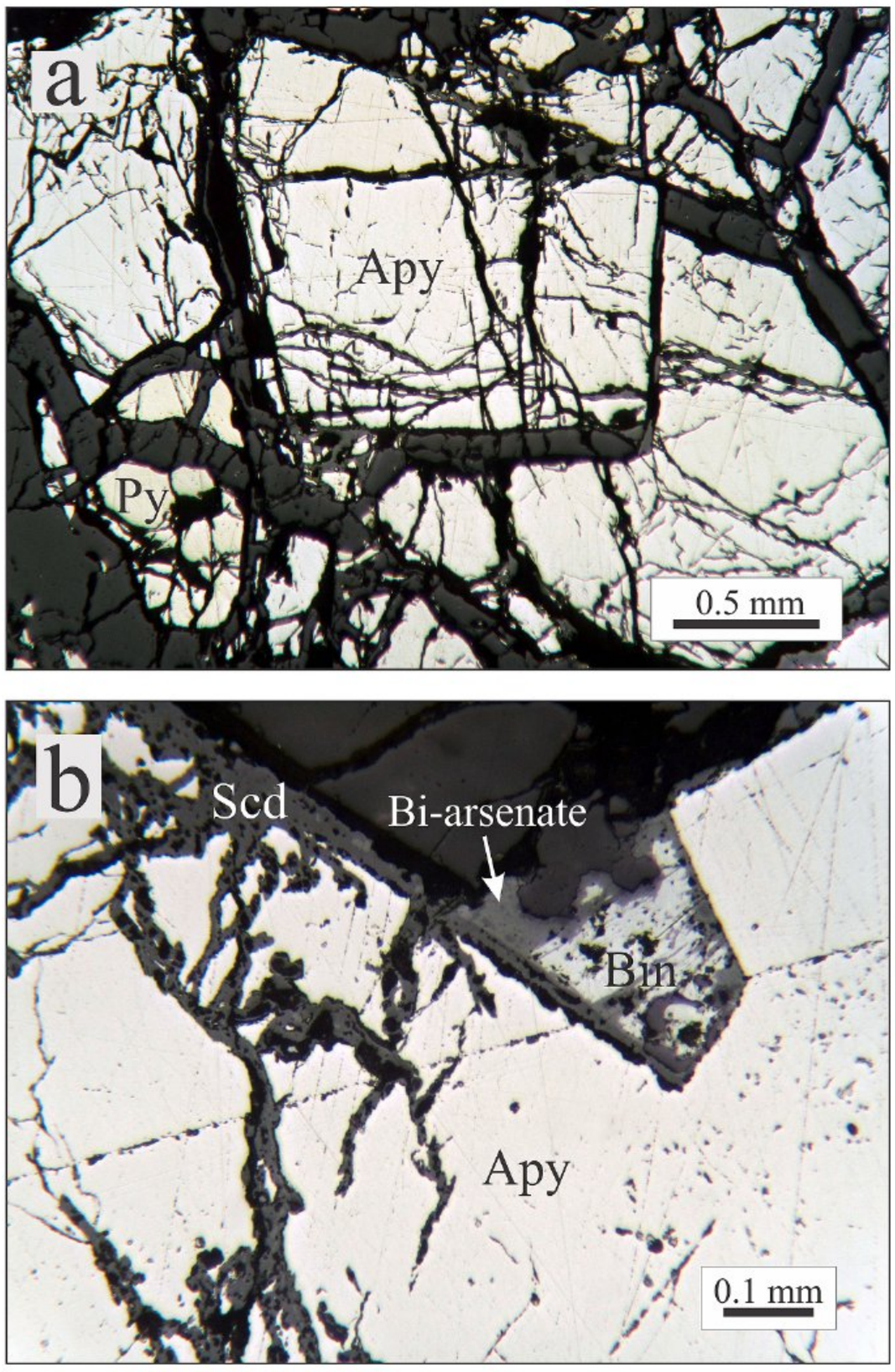

Fig. 2. a-b. Mineral assemblage of the studied mineralization generally consists of arsenopyrite (Apy), pyrite (Py), bismuthinite (Bin), scorodite (Scd) and quartz (dark gray gangue). Scorodite contains fine-grained Bi-arsenate replacing bismuthinite (Sample T1-5, reflected light, air, //N).

fine grains up to 0.1 mm in size. Native bismuth that forms fine grains mostly up to 30 μm, rarely to 0.1 mm in size, often occurs in association with bismuthinite. Its presence is significant because most of the gold (*I generation*) was deposited in close association with native bismuth and bismuthinite, filling the microcracks in arsenopyrite (Fig. 5d-f). In that manner, dozens of fine grains of gold and Bi minerals can be found even within one oxidized arsenopyrite grain, healing its cavities and microcracks (Fig. 7). Thus, it can be reliably said that gold was later deposited relative to its host arsenopyrite. Tens of SEM-EDS analyses of this gold showed the presence of silver, mainly in the range of 4–10 wt% Ag.

Stage 3 involves the oxidation of sulfides and the formation of scorodite and Bi-arsenate, which represent the last mineral deposition event in the studied mineralization. Scorodite was mainly formed by arsenopyrite replacement, but this mineral has also cemented other main constituents quartz and pyrite (Fig. 3b). It is unevenly distributed and generally follows the mineral assemblage of the second stage, in addition to the predominant arsenopyrite and quartz from the first stage of deposition. Scorodite is generally considered a weathering product of arsenopyrite and other As minerals. However, in the case of the Drenjak it is not so obvious, and this topic will be one of the subjects of upcoming discussion. Minor amounts of Bi-arsenate replacing bismuthinite, often occur in close association with scorodite (Fig. 2b), but in such fine μm-sized grains (e.g. Fig. 6c,d), which cannot be fully identified. Scorodite and subsidiary Bi-arsenate readily host fine gold grains (Figs. 5-7). Most of these grains represent relict gold (*I generation*) retained after the oxidation of the sulfides. However, scorodite and Bi-arsenate often contain finely dispersed micrometre to sub-micrometre gold grains that cannot be clearly determined as relict grains or the grains which are co-precipitated with these arsenates (e.g. Fig. 6c,d). Such gold extends the above-mentioned range of silver content toward lower values, and even Ag-free gold grains are common in scorodite. No correlation was established between the size of the gold grains and Ag content, nor the spatial distribution of gold with different concentrations of silver. Silver-bearing and silver-free gold grains even coexist in scorodite (Fig. 6c,d). However, the occurrence of open-space filling colloidal-like gold finely dispersed in Bi-arsenate and scorodite present in the microcracks in arsenopyrite (Fig. 7d), which somewhere resembling to colloform gold (Fig. 5f), must have been precipitated simultaneously with the arsenates, forming the *II generation* of gold.

4.2. TEM study

Given that gold in arsenopyrite and scorodite occurs in very fine grains that are often near and probably below the resolution limit of a polarized-light microscope and SEM, TEM investigation was further used to determine the possible presence of gold also on the nanometer scale. TEM study was applied to one representative gold-bearing grain of partly oxidized arsenopyrite, shown in Fig. 7a.

First, arsenopyrite is found in large single-crystal domains. The cell parameters calculated from the SAED pattern (Fig. 8) show no deviation from the prototype structure (Bindi et al., 2012). The chemical composition analysed by EDS spot-analysis corresponds to stoichiometric FeAsS. The microcracks and fissures in arsenopyrite are abundant, and some of them are filled with polycrystalline μm- to nm-sized gold, consisting of nanocrystallite 20–30 nm in size (Fig. 8c,d). Upon closer look, the Au phase is not entirely dense, and several voids between the crystallites are still visible. The individual Au nanocrystallites are randomly oriented, and most of them show characteristic ∑3-type twin lamellae (s.c. spinel-type twinning). The contact between Au nanocrystallites and host arsenopyrite is rather sharp, without any intermediate phases and arsenates on the phase interface. From the observed details, it is safe to assume that this gold was deposited after the mechanical fracture of arsenopyrite and before the oxidation process took place.

4.3. Scorodite features

Studied scorodite generally occurs as cryptocrystalline aggregates that replace arsenopyrite and cement quartz and pyrite, frequently forming fine crusts less than 0.5 mm thick. It is white in color with a greenish tint that is often seen on the samples (Fig. 1e). Over ten SEM-EDS analyzes showed the only presence of sulfur as a trace element, in relatively uniform concentrations from 0.5 to 1 wt% S. XRD analysis (Fig. 4) confirms the identification of this Fe-arsenate as scorodite, given that in nature it is possible to form its dimorph parascorodite, as well as the amorphous phases of this composition and iron sulfo-arsenate. Additionally, sharp peaks on the diffractogram confirm its good crystallinity. The morphology of scorodite was further examined by SEM. On that occasion, a transition from a botryoidal-like texture (Fig. 9a) to plate-like aggregates forming the clusters (Fig. 9b) was discovered on the micrometre scale.

4.4. Trace elements in sulfides

The main goal of trace element analysis in sulfides is to determine whether gold is present in an elevated content, primarily in arsenopyrite. Trace element contents in arsenopyrite and pyrite are given in Table 1. Arsenopyrite occasionally shows slight compositional zoning on back-scattered electron images, mainly caused by the elevated contents of Co (up to 2.3 wt%) and Ni (up to 0.3 wt%). On the other side, pyrite

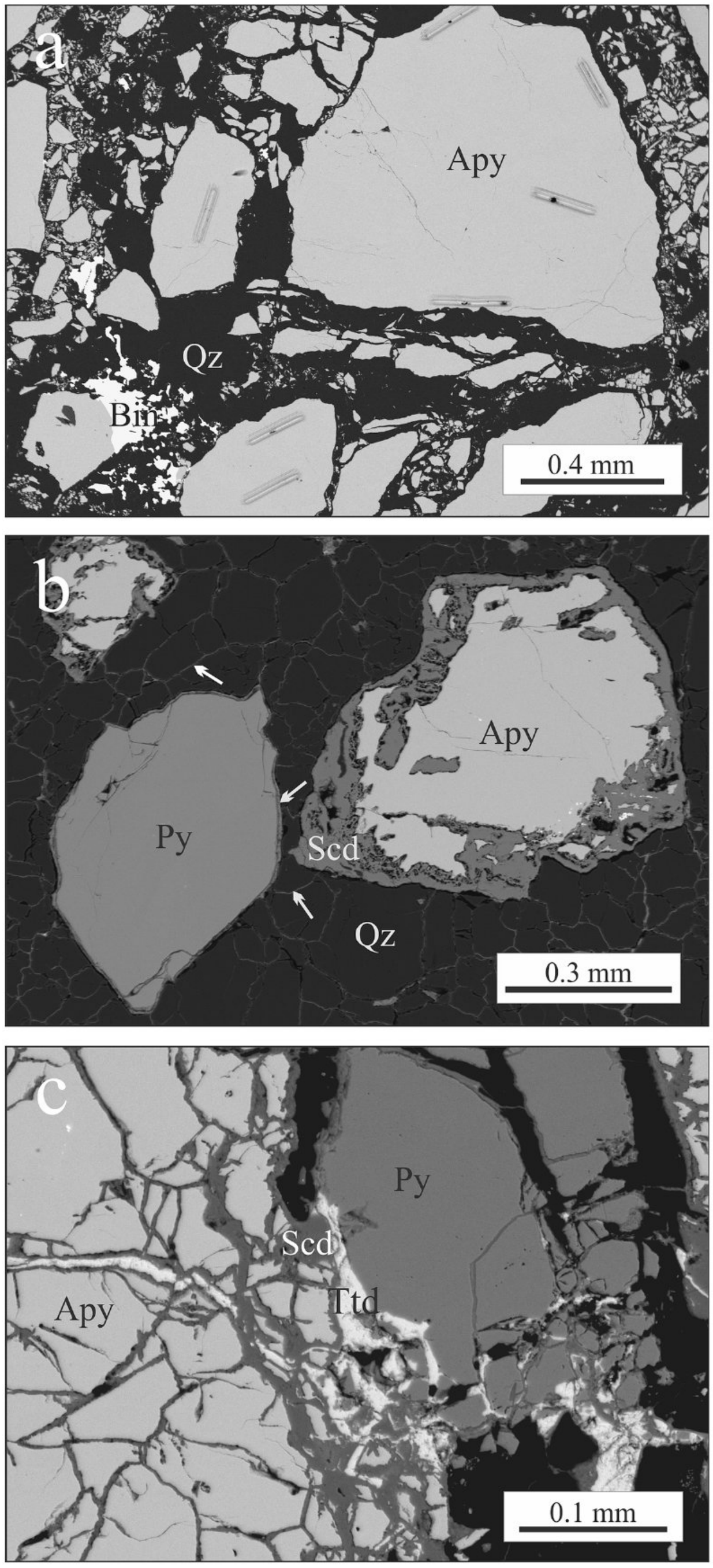

Fig. 3. Varying presence of scorodite in the mineralization (BSE images). **a.** Paragenesis of the first stage of deposition consisting of arsenopyrite (Apy), quartz (Qz) and bismuthinite (Bin) from gold-free sample T1-1. Note the absence of scorodite. Line-raster pits of LA-ICP-MS analysis in arsenopyrite can be also noted. **b.** Previously mentioned minerals from the first stage were replaced and cemented by scorodite (Scd) in gold-bearing sample T1-2. Fine cementation of pyrite and quartz along the grain rims and cracks is highlighted by arrows. Note the obvious textural difference of quartz in Figs. a and b caused by scorodite absence/presence in the samples. **c.** Arsenopyrite and pyrite are cemented by scorodite and tetrahedrite (Ttd) assemblage (sample T1-2).

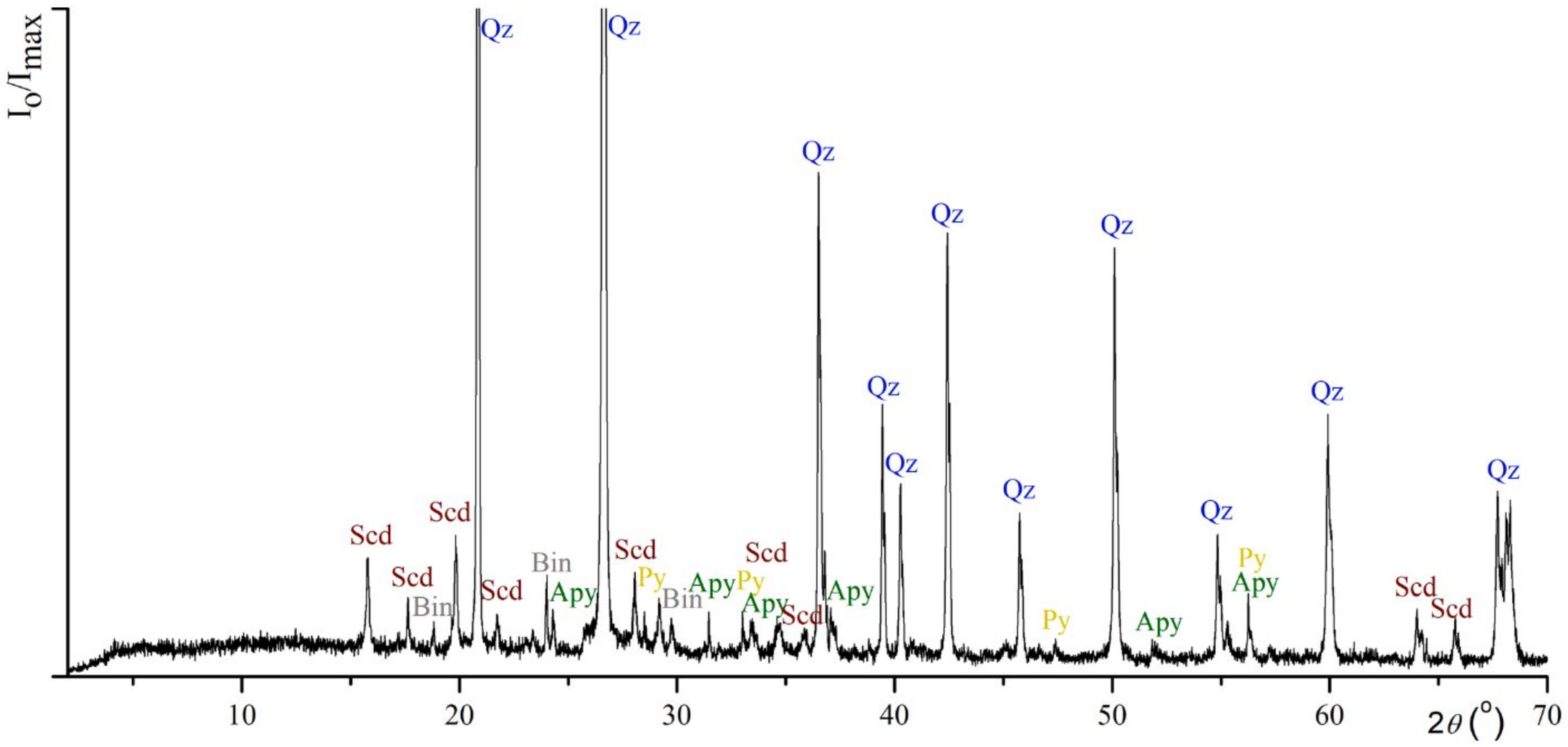

Fig. 4. XRD pattern of sample T1-2 shows the presence of well-crystallized scorodite (Scd) among principal minerals in the sample quartz (Qz), arsenopyrite (Apy), pyrite (Py) and bismuthinite (Bin). The two most intense peaks of quartz are cut off.

shows no apparent compositional zoning. Arsenic is the major trace element in this mineral and shows a fairly uniform concentration (except for one analysis) in the range of 0.7–1.0 wt% As.

Excluding the contents which surely come from the inclusions, gold concentration in arsenopyrite and pyrite reaches only 5.2 ppm. There are no obvious differences in Au contents in arsenopyrite from samples with and without visible gold grains. Also, no possible Au-Bi correlation in arsenopyrite was established, except in the case of previously mentioned contents from the subsurface and/or submicroscopic inclusions. Bismuth content in arsenopyrite ranges from 0.3 to 92.9 ppm, while highly elevated values correlate with the Bi-bearing inclusions. A limited number of analyses show that Bi content in pyrite does not exceeds 0.52 ppm. It is worth noting that silver concentrations ($\leq$0.47 ppm) in arsenopyrite and pyrite are much lower than gold contents ($\leq$5.2 ppm).

Further trace element content in arsenopyrite is fairly homogeneous: Sb is present in concentrations mostly of a few hundreds of ppm, Se and Te contents fluctuate mostly in the range of tens of ppm, while Mn, Cu, Ge and In show pretty uniform contents in the range of 1–10 ppm. Lead shows contents of a few ppm in some analyses but is more often below 1 ppm, similarly to zinc (not shown in the table) and cadmium. Poor negative Sb-Cu and positive Co-Ni correlations were observed.

Comparing the trace element contents of coexisting arsenopyrite and pyrite from sample T1-2, preferential enrichment of Co and Sb in arsenopyrite is first observed. Although, it is well-known that arsenopyrite readily incorporates these two elements, forming the solid solutions towards glaucodot (Co,Fe)AsS and gudmondite FeSbS, respectively. However, it can be noticed that several other traces like Se, Te, In and Bi also prefer arsenopyrite structure.

Trace elements in sporadic to minor sulfides bismuthinite and tetrahedrite were analyzed only by two LA-ICP-MS analyses. Bismuthinite from sample T1-1 showed gold content of 1.8 and 5 ppm and elevated silver content of 3–16 ppm compare to major sulfides. Gold and bismuth concentration in tetrahedrite from sample T1-2 is even below 0.2 ppm and as high as 33 ppm, respectively. The silver content in tetrahedrite up to 995 ppm is not surprising, having in mind that this mineral is often enriched by silver even in the range of wt.%.

5. Discussion

5.1. Hydrothermal versus weathering origin of scorodite

As stated in the introduction, the origin of scorodite in nature is related only to weathering processes. Also, Bi-arsenates (rooseveltite and its dimorph tetrarooseveltite, $Bi(AsO_4)$, atelestite, $Bi_2(AsO_4)O(OH)$, preisingerite, $Bi_3(AsO_4)_2O(OH)$) representing rare minerals in nature, are described as weathering phases (e.g. Bedlivy and Mereiter, 1982, Sejkora et al., 2006, Frost et al., 2011). Therefore, scorodite and subsidiary Bi-arsenate from the Drenjak should be typical weathering minerals, according to the literature survey. The cryptocrystalline nature of scorodite supports this interpretation.

Despite the above facts, we draw attention to the possibility of a hypogene, low-temperature hydrothermal origin of scorodite (and Bi-arsenate) from the studied mineralization, based on the following evidence:

1. It is unlikely that arsenopyrite was weathered while coexisting pyrite was not affected by the same process (e.g. Fig. 3b). Common products of pyrite weathering alteration - limonite, goethite, etc, or possible formation of sulfate (e.g. jarosite) depending of depositional conditions, are absent in all studied samples even in negligible amounts. Numerous studies confirm that scorodite is associated with the alteration products of pyrite, when arsenopyrite-pyrite assemblage was affected by the weathering alteration (e.g. Salzsaueler et al., 2005, Walker et al., 2009, Murciego et al., 2011).
2. The occurrence of gold and elevated amounts of Bi minerals correlates with the presence of scorodite in mineralization. If this Fe-arsenate has a weathering origin, the question arises why this Au-Bi assemblage of hydrothermal origin associates with scorodite.
3. The close association of tetrahedrite and scorodite filling the cracks in arsenopyrite and pyrite (Fig. 3c) indicates that these two minerals were deposited from the same solution. And, tetrahedrite is known only as a hydrothermal mineral.
4. Finally, artificial scorodite is often obtained by hydrothermal synthesis (Dove and Rimstidt, 1985, Krause and Ettel, 1988, Singhania et al., 2005, Xu et al., 2007, Gomez et al., 2010). It means that its stability field expands towards elevated temperatures of aqueous

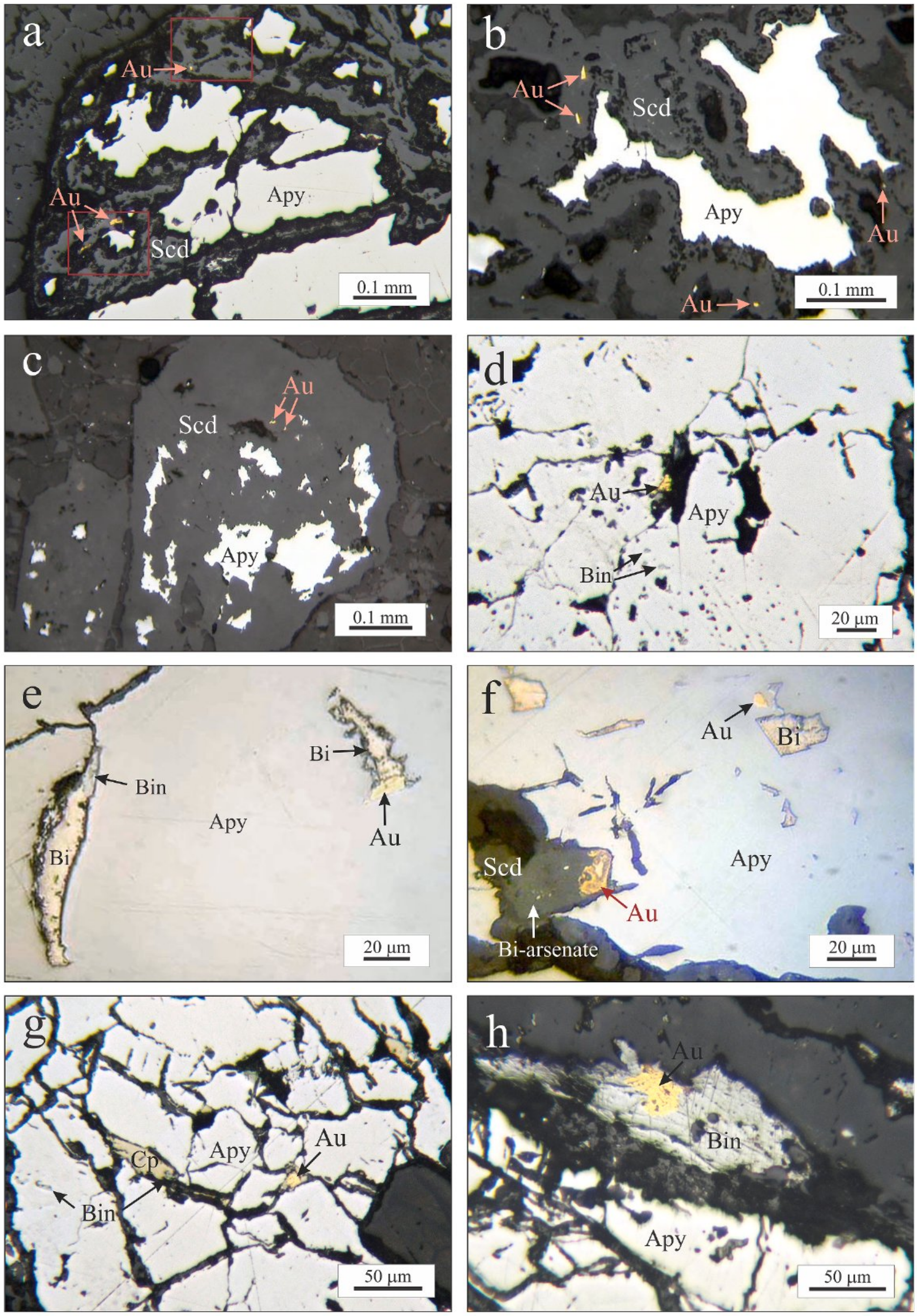

Fig. 5. Gold occurrence in the studied mineralization (reflected light, air, //N). a-c. Gold (Au) that is hosted by scorodite (Scd) replacing arsenopyrite (Apy) (sample T1-2). Rectangles in (a) mark close-ups shown in Fig. 6c,d, respectively. d-f. Gold (Au) mainly located in the cavities and microcracks of arsenopyrite (Apy). It often closely associates with native bismuth (Bi) and bismuthinite (Bin) (d – sample T1-6, e,f - sample T1-5; image in (f) is taken from Pačevski, 2002). Note colloidal-like gold resembling to colloform texture (marked by red arrow), located in the microcrack of arsenopyrite filled out by the scorodite (Scd) and Bi-arsenate. g. Gold (Au) that is located in the microcrack of arsenopyrite (Apy), associates with chalcopyrite (Cp) and bismuthinite (Bin) (sample T1-6). h. Occurrence of gold (Au) in bismuthinite (Bin) (sample T1-7).

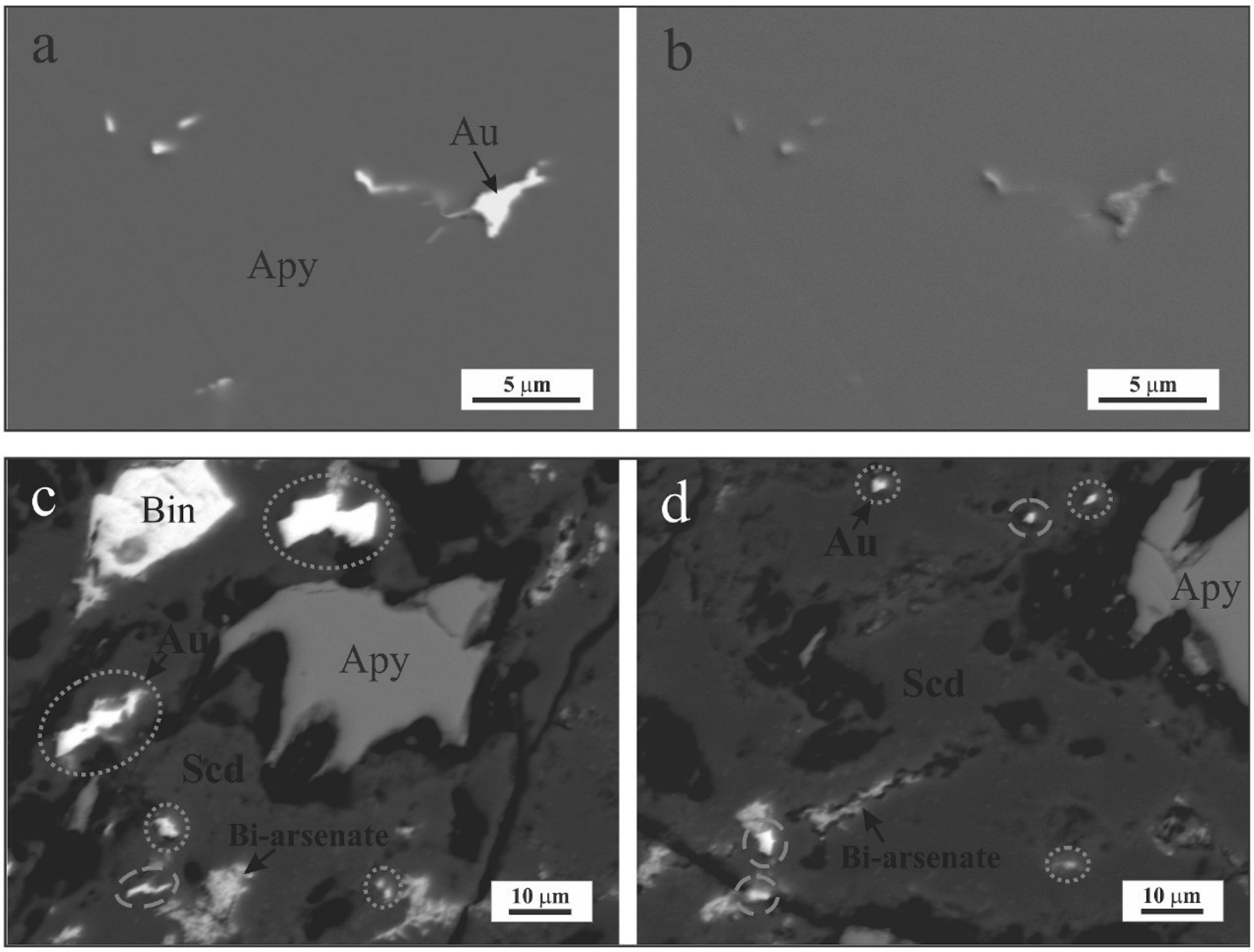

Fig. 6. Occurrence of gold in arsenopyrite and scorodite with the grain size close to the resolution limit of SEM method (a,c,d – common BSE images; b – BSE image in TOPO mode). **a-b.** Gold (Au) in arsenopyrite (Apy). Topography given in (b), shows "the pits" in the position of gold grains. Such topography in the polished section causing an effect of emerging glow, appears due to the high difference in the hardness between gold and host arsenopyrite. **c**, **d.** Numerous gold (Au) grains (5 grains in fig. c and 6 in d) hosted by scorodite (Scd). The grains are highlighted by circles; grains of pure gold by dotted circles, while those with silver content (up to several wt.% Ag) by the interrupted lines. These two figures represent close-ups marked by rectangles in Fig. 5a, and arsenopyrite (Apy), bismuthinite (Bin) and Bi-arsenate are also present here.

solutions. In that case, why cannot it form from low-temperature ascending solutions at the end of the hydrothermal activity? For this reason, we would like to point out the need for upcoming research, which also includes the occurrence of scorodite in nature, to be directed in this direction as well.

5.2. *Formation of colloidal-like gold in scorodite*

The μm-sized gold grains in scorodite can be easily explained as inclusions formed by an earlier depositional process (*I generation* of gold). On the other side, the colloidal-like gold occurring with Bi-arsenate in scorodite (Fig. 5f, 7d; *II generation*), are definitely co-genetic with these arsenates. Therefore, it seems that the oxidation process of arsenopyrite partly also affected the gold grains located in the microcracks of this sulfide.

It is well-known that gold is released from sulfides during their oxidation. Solubility of such gold in various crustal, especially weathering solutions, has been of particular interest and the subject of many studies in the past (e.g. Stokes, 1906, Boyle et al., 1975, Stoffregen, 1986, Kalinin et al., 2009, Craw et al., 2015). For example, Boyle et al. (1975) summarized that gold could be transported in supergene solutions in various compounds, including iron sulfate solutions in the case where pyrite, pyrrhotite, arsenopyrite and other sulfides are oxidized. These authors also noted that gold solubility is higher when released from fine "invisible gold" in arsenopyrite and other Au-bearing minerals than from larger μm-sized grains. Further, Bowell (1992) explained that gold is released from the hypogene orebody by physical disaggregation and chemical dissolution and that the dissolution and reprecipitation appears to take place mainly in situ.

Thus, our proposition of the formation of colloidal-like gold, playing out during the sulfide oxidation, agrees with the earlier studies. Moreover, the nanocrystalline nature of relict gold can intensify the processes of physical disaggregation and chemical dissolution of gold, and even formation of gold nanoparticles similar to that reported by Hough et al. (2011) can be expected. Assuming that the same or similar mechanism of sulfide oxidation and gold release occurs not only from supergene but also from low-temperature ascending solutions, the uncertainty regarding the hydrothermal or weathering origin of scorodite given in previous section does not question this interpretation.

However, in addition to the previous suggestion of colloidal-like gold formation, another possibility should be considered. Namely, gold is known to exist in hydrothermal solution down to low temperatures, for example, in the case of epithermal gold systems (e.g. Saunders, 1990). Thus, besides previously determined relict gold (*I generation*) in scorodite, additional Au-enrichment of this mineral directly from the solution (*II generation* of gold) can be expected. This assumption should be taken into account only if scorodite was indeed formed from a hot ascending solution at the end of the hydrothermal stage, which we present as one possibility in previous section. This assumption is also supported by the observed correlation in the presence of the Au-Bi

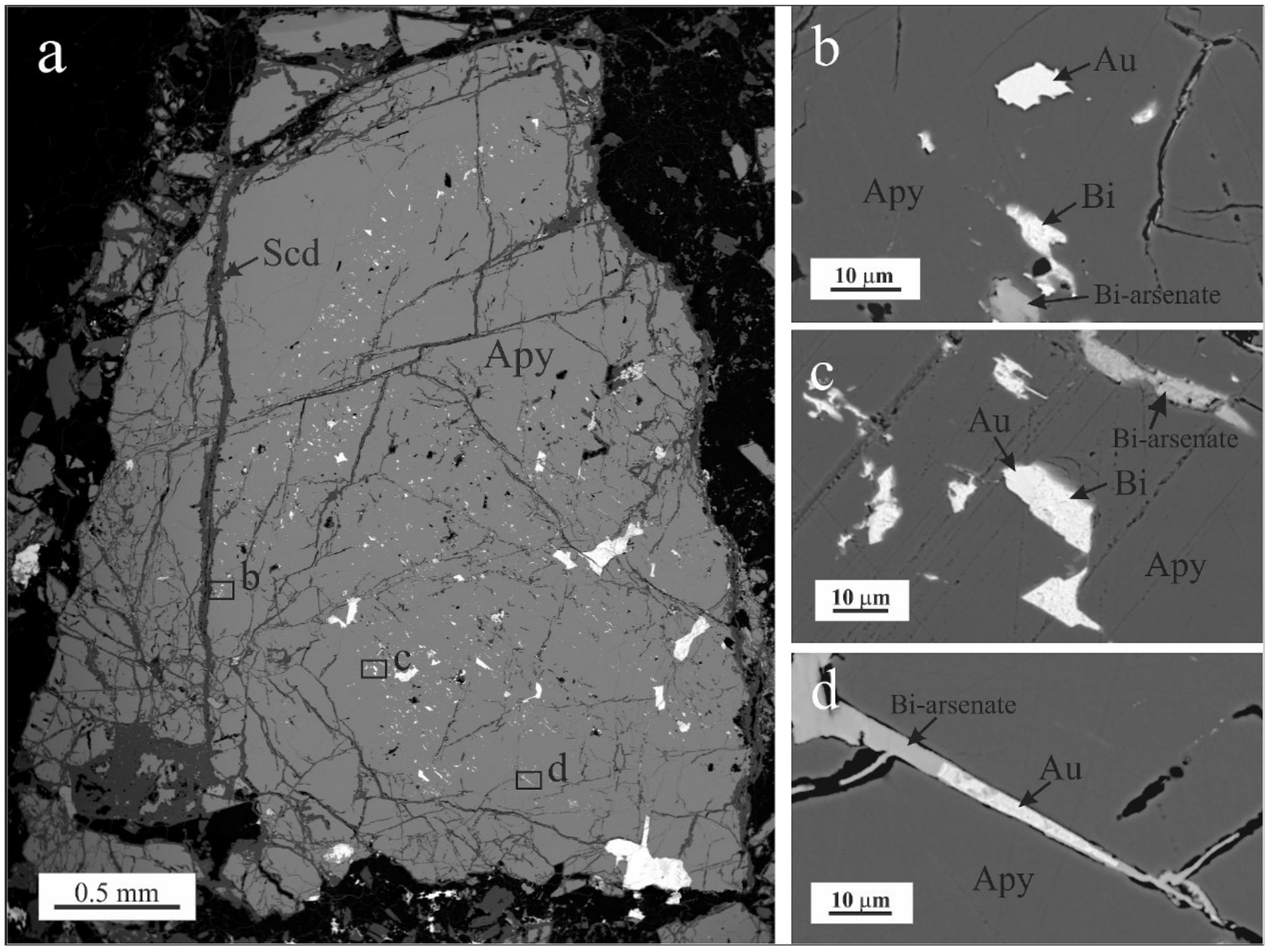

Fig. 7. **a**. Representative arsenopyrite (Apy) grain containing dozens of fine grains of Bi minerals and gold (white grains; Bi minerals predominate) from sample T1-2. It is replaced by scorodite (Scd) along the cracks. Rectangles labeled by b-d mark the positions of close-ups shown in figs. b-d, respectively. **b**. Gold (Au) grain in arsenopyrite detached from Bi minerals - native bismuth (Bi) and Bi-arsenate. **c**. Coalescence of gold with native bismuth. **d.** Gold in Bi-arsenate fills the crack of arsenopyrite, along with scorodite (black parts, due to decreased brightness of BSE image).

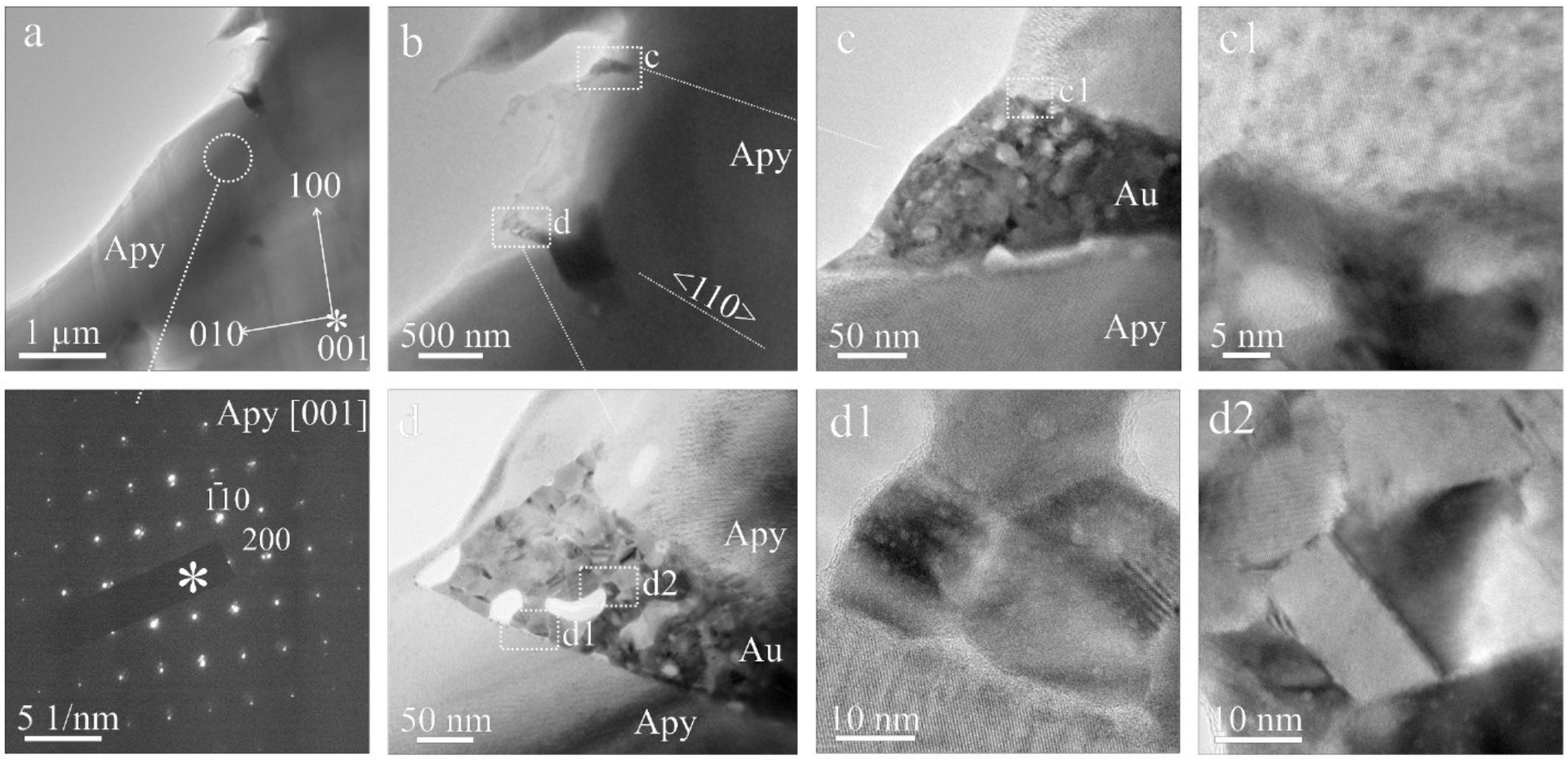

Fig. 8. **a.** Overview TEM micrograph of large arsenopyrite crystal from Fig. 7a, with marked Au-filled microcracks, and corresponding SAED. **b.** magnified Au-rich zones. **c, d.** Polycrystalline gold consists of nanocrystallites and forms sharp contact with host arsenopyrite.

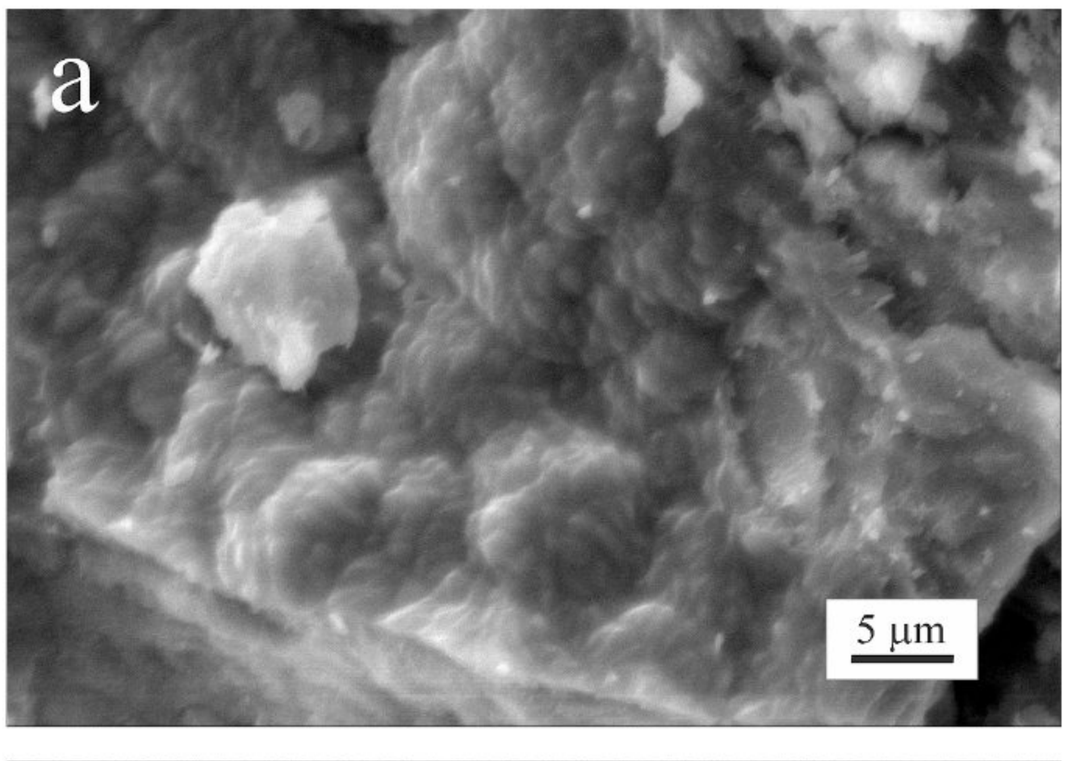

Fig. 9. Morphology of scorodite on the fracture surface of sample T1-2 (SE images).

mineral assemblage with scorodite in the studied mineralization.

5.3. Depositional evolution

In hydrothermal fluids, arsenic is mainly transported as As(III), forming hydroxide and sulfide complexes (Ballantyne and Moore, 1988, Pokrovski et al., 1996, and references therein). Arsenopyrite is the ubiquitous As-bearing mineral in various high-temperature to mesothermal hydrothermal deposits. Its formation conditions correspond to a temperature range from ~ 250 °C to 500 °C, and this mineral generally controls As transport and deposition from high-temperature (>300 °C) fluids (Pokrovski et al., 2002, and references therein). At lower temperatures (<300 °C) arsenian pyrite is a common As-bearing mineral in meso- and epithermal sulfide deposits of gold (e.g. Ballantyne and Moore, 1988, Fleet et al., 1989, 1993, Mumin et al., 1994). According to these data, we can roughly estimate that our first stage of deposition mainly composed of arsenopyrite and pyrite containing ≤ 1 wt% As, was formed from a hydrothermal solution of higher temperature (>250 °C).

Gold in the ore deposits can readily be found in arsenopyrite. For example, Hinchey et al. (2003) reported Au concentration in arsenopyrite attaining 201 ppm, and Sung et al. (2009) measured by LA-ICP-MS up to 5767 ppm. Tremendous studies on this topic reported the highest concentrations of gold, detectable even by EMPA; in arsenian pyrite up to 3,700 ppm (Fleet and Mumin, 1997), and in arsenopyrite up to 4,400 ppm (Cabri et al., 1989), 4,700 ppm (Genkin et al., 1998) and even to 13000 ppm, i.e. 1.30 wt% (Cook and Chryssoulis, 1990). However, gold content in arsenopyrite and other sulfides from our mineralization reaches only 5 ppm. Therefore, there is no elevated gold content in arsenopyrite and other sulfides which would be released and remobilized by the oxidation of these sulfides.

Numerous studies describe the existence of "invisible gold" in arsenian pyrite and arsenopyrite as a consequence of various depositional growth mechanisms (Genkin et al., 1998, Cabri et al., 2000, Palenik et al., 2004, Reich et al., 2005, Sung et al., 2009, Cook et al., 2013, Fougerouse et al., 2016). On the other side, in many vein deposits containing arsenopyrite, gold precipitation occurs later than the formation of arsenopyrite ± pyrite (Heinrich and Eadington, 1986, Genkin et al., 1998). This last case completely coincides with the occurrence of gold healing the arsenopyrite microcracks in the Drenjak mineralization. Thus, major portion of gold (*I generation*) is deposited after arsenopyrite crystallization, most probably at a medium to low temperature hydrothermal stage.

This generation of gold is almost regularly associated with bismuthinite and native bismuth, clearly indicating an Au-Bi correlation. At the same time, native bismuth and gold frequently show mutual coalescence, and according to this assemblage, it can be suggested that gold was partly scavenged from hydrothermal solution by bismuth melt. Bismuth is distinguished by its low melting point of 271.4 °C. Above this temperature, Bi-rich melts can coexist with aqueous fluids. Such hydrothermal fluids (200–400 °C) may contain polymetallic melts (e.g. Bi-Au), which probably have a more significant role in ore enrichment than currently recognized (Tooth et al., 2008). The experiments and calculations on the partitioning of gold between a hydrothermal solution and bismuth melt demonstrated that Au concentration in the melt was several orders of magnitude higher than in the coexisting fluid (Douglas et al., 2000, Tooth et al., 2008). These authors further indicated the possible formation of economic gold deposits from undersaturated hydrothermal fluids in which mineralization would not be expected without a bismuth melt.

According to Au-Bi binary phase diagram, an Au-Bi melt can exist down to the eutectic temperature of 241 °C with 19 wt% Au when maldonite (Au_2Bi) and native bismuth started to crystallize (Tooth et al., 2008). These authors further presented an example from Maldon (Australia) of the coexistence of these two minerals representing the eutectic association formed at the mentioned temperature. The same ore was also described by Ciobanu et al. (2010), who pointed out that these two minerals crystallized from melt droplet inclusions, but in the hydrothermal stage and exhibited decomposition textures. In the case of our mineralization, maldonite was not formed with native bismuth, than gold. In addition, these gold-bismuth grains, filling the microcracks and pores in arsenopyrite (Fig. 5e and 7c), do not show rounded shapes typical for melt droplet inclusions. In the Au-Bi binary phase diagram of Tooth et al. (2008), the absence of maldonite and coexistence of only native bismuth and native gold is in the stability field below temperature ~ 116 °C. They explained the partial decomposition of previously mentioned maldonite from its type locality into symplectites of native Bi and Au during cooling below this temperature. Although no appearance of dissolution of a solid solution or any other distinctive texture has been recorded, fine gold-bismuth grains in the mineralization of Drenjak were probably also deposited from a lower temperature solution, certainly below 271.4 °C (melting point of Bi).

Simultaneously with temperature decreasing, other physic-chemical changes took place during the hydrothermal evolution, which led to the partial dissolution and replacement of arsenopyrite in the studied mineralization. The direction of these changes is traced by the occurrence of tetrahedrite, i.e. a member of the tetrahedrite-tennantite series in the next depositional stage (Fig. 3c). Compared to arsenopyrite, the tetrahedrite-tennantite solid solution was formed at a lower temperature and the most probably from f_{O2}-elevated solutions. Namely, Einaudi et al. (2003) showed that arsenopyrite forms in conditions of the low-sulfidation state, while tennantite is in a higher, intermediate sulfidation state of a fluid. They also discussed the relationship between sulfidation and oxidation states and mentioned that f_{O2} covaries with f_{S2}. In addition, arsenic in arsenopyrite is present as an anion, most likely as As^{-1} (e.g. Jones and Nesbitt, 2002), while in tennantite it is cation As^{3+}.

Table 1
LA-ICP-MS trace element data for principal sulfides arsenopyrite (Apy) and pyrite (Py) from the Drenjak (in ppm). Arsenopyrite was analyzed in four samples; two samples containing fine gold grains (T1-2 and T1-5) and the other two without revealed gold (T1-1 and T1-3). Content of elements that most likely originate from fine inclusions are marked by sign "*" and is excluded from the calculation of a mean value.

	Mn	Co	Ni	Cu	Ge	Se	Ag	Cd	In	Sb	Te	Au	Bi	Pb	As
T1-1 (Apy)															
81	1.9	620.0	12.5	2.4	2.2	10.3	0.10	0.22	3.3	57.0	35.9	3.3	9.6	0.53	
2	1.5	337.2	471.0	2.2	2.2	5.8	0.16	0.27	3.3	42.6	7.7	2.7	12.3	1.79	
3	1.4	622.0	42.9	2.1	1.9	7.0	0.06	0.27	3.5	46.7	22.6	5.2	2.1	0.58	
4	1.6	435.9	797.1	2.6	2.1	6.9	0.07	0.26	3.4	49.6	12.8	2.8	4.7	0.90	
5	1.5	2906.4	308.8	1.9	2.1	5.5	0.07	0.18	3.6	45.7	4.2	1.7	8.4	0.59	
6	1.7	711.7	263.0	1.5	2.2	5.9	0.05	0.21	3.5	50.0	5.1	2.3	4.5	0.49	
7	1.5	22785.6	3101.5	2.1	3.0	60.8	0.15	0.24	3.8	76.8	36.9	1.4	92.9	0.48	
mean	*1.6*	*4059.9*	*713.8*	*2.1*	*2.3*	*14.6*	*0.09*	*0.24*	*3.5*	*52.6*	*17.9*	*2.8*	*19.2*	*0.76*	
T1-2 (Apy)															
1	1.4	109.3	6.8	1.3	1.8	9.1	0.06	0.20	3.1	204.8	20.5	0.50	4.9	0.16	
2	1.2	98.5	13.9	1.8	1.9	16.9	0.06	0.16	3.1	467.0	31.8	0.13	8.49	0.18	
3	1.6	63.8	2.7	1.0	2.0	14.7	6.26*	0.23	3.2	313.0	15.7	52.0*	6585.9*	1.39*	
4	1.4	39.8	3.4	0.7	1.9	13.7	0.11*	0.28	2.9	273.3	2.8	0.86*	636.3*	0.18	
5	1.3	90.3	27.6	0.6	1.9	11.1	0.07	0.17	2.9	259.9	4.8	0.27	88.1	0.11	
6	1.4	109.0	10.6	1.3	1.9	13.4	0.05	0.18	2.8	253.2	10.8	0.13	24.0	0.27	
7	1.2	136.5	505.3	2.7	2.0	12.9	bdl	0.21	3.6	259.1	33.3	0.31	3.3	0.26	
8	1.1	160.5	35.6	0.9	2.1	11.4	0.06	0.25	3.6	243.7	14.0	0.26	10.9	0.16	
9	1.2	94.1	9.9	1.8	1.9	12.2	0.03	0.23	3.6	270.0	4.1	0.30	7.1	0.32	
mean	*1.3*	*100.2*	*68.4*	*1.3*	*1.9*	*12.8*		*0.21*	*3.2*	*282.7*	*15.3*	*0.27*	*20.9*	*0.33*	
T1-2 (Py)															
1	2.0	0.2	432.3	1.5	1.3	4.9	bdl	bdl	0.10	bdl	bdl	2.8	0.52	0.23	9545.5
2	1.9	7.8	8.8	2.1	1.5	3.7	bdl	bdl	bdl	bdl	bdl	bdl	0.12	0.12	258.2
3	2.0	0.1	31.5	1.5	1.6	6.5	bdl	bdl	0.10	bdl	bdl	1.2	0.10	0.11	9855.8
4	1.9	0.1	93.6	1.7	1.6	6.3	bdl	bdl	0.10	bdl	bdl	1.9	0.26	0.12	9733.6
5	2.0	0.1	3.9	1.2	1.5	5.0	bdl	bdl	0.05	bdl	bdl	0.2	0.04	0.07	6817.9
mean	*2.0*	*1.7*	*114.0*	*1.6*	*1.5*	*5.3*							*0.21*	*0.13*	*7242.2*
T1-3 (Apy)															
1	5.1	102.0	61.7	8.3	2.6	10.7	bdl	bdl	3.1	62.3	0.7	0.63	3.8	0.8	
2	2.3	3582.9	1754.6	3.2	2.1	13.5	bdl	bdl	3.5	200.9	45.8	bdl	2.5	0.8	
3	2.9	921.1	904.8	6.4	2.0	11.4	bdl	bdl	3.5	61.9	4.0	bdl	13.1	3.3	
4	2.5	788.2	786.6	7.0	2.5	12.3	bdl	bdl	3.5	65.5	6.2	bdl	1.1	1.3	
5	3.4	1391.1	471.0	5.4	2.3	11.4	bdl	bdl	3.4	134.3	9.8	0.25	3.5	1.5	
6	2.2	59.8	10.0	4.9	2.4	10.3	bdl	bdl	3.3	172.2	1.0	bdl	0.3	1.2	
7	3.3	754.4	85.7	3.1	2.6	16.6	bdl	bdl	3.4	140.7	17.1	bdl	0.8	0.6	
mean	*3.1*	*1085.6*	*582.1*	*5.5*	*2.4*	*12.3*			*3.4*	*119.7*	*12.1*		*3.6*	*1.4*	
T1-5 (Apy)															
1	1.3	7221.0	309.5	0.9	2.2	67.5	bdl	0.12	3.4	101.7	72.4	0.20	5.8	0.1	
2	1.5	2080.9	591.8	16.4	2.1	18.7	0.17	0.27	3.3	48.0	13.1	1.98	16.1	2.5	
3	2.0	2445.5	195.7	2.7	2.6	46.0	bdl	0.24	3.3	88.3	51.3	0.14	5.4	0.4	
4	1.4	965.5	176.2	2.4	2.7	41.6	bdl	0.24	3.5	163.0	53.5	0.27	4.8	0.4	
5	1.9	5375.0	205.5	1.1	2.2	31.3	bdl	0.26	3.4	237.9	24.9	0.09	3.4	0.1	
6	1.3	911.2	80.4	1.1	2.7	29.8	0.76*	0.20	3.4	45.0	95.1	183.7*	2771.6*	1.7	
7	1.9	1282.9	37.9	4.3	1.9	8.5	0.47	0.18	3.4	68.4	6.3	2.64	24.9	3.0	
mean	*1.6*	*2897.5*	*228.1*	*4.1*	*2.3*	*34.8*		*0.22*	*3.4*	*107.5*	*45.2*	*0.89*	*10.1*	*1.8*	
dl	1.0	0.05	2.2	0.50	0.40	3.6	0.03	0.11	0.04	0.12	0.10	0.20	0.04	0.10	133

bdl – below detection limit; dl – detection limit; blank – principal element in a mineral.

The replacement of tetraedrite-tennantite member by scorodite could indicate a further increase in f_{O2} and the formation of arsenates (scorodite and Bi-arsenate) at low temperature.

5.4. As-Au-Bi assemblage

The close association of native gold with Bi minerals and its often intergrowth with native bismuth is one of the main characteristics of the studied mineralization. This fine-grained mineral assemblage was almost always hosted by arsenopyrite and its product of oxidation scorodite (Figs. 5-7), forming an As-Au-Bi assemblage. For example, pyrite, which is the second main sulfide in the mineralization, does not contain Au and Bi minerals even to the smallest extent. However, the connection of this Au-Bi assemblage with the arsenic mineral substrate has not yet been elucidated.

As suggested by Heinrich and Eadington (1986) and emphasized by Pokrovski et al. (2002), native gold deposition on grain boundaries and in cracks of arsenopyrite is likely to be explained by the minor dissolution of arsenopyrite, a process that would act as a local redox trap for gold. Their prediction is consistent with the selective reduction of Au^{3+} to Au^0 on the arsenopyrite surface, which has been demonstrated in some studies (Möller and Kersten, 1994; Fleet and Mumin, 1997; Madox et al., 1998). Partial dissolution of arsenopyrite from Drenjak is evident due to the presence of scorodite. Thus, the process of local redox trap for gold at least partly directs its deposition in arsenopyrite cracks/cavities, forming an As-Au correlation. We should not forget the previously described Au-Bi correlation in this mineralization. Finally, we suggest that the existence of As-Au-Bi system is the result of the coupling of two processes; i) local redox trap for gold (and way not Bi) on arsenopyrite and, ii) association of gold to bismuth in the solution, partly through the scavenging process.

6. Conclusions

In the mineralized quartz bodies at Drenjak, three depositional stages have been determined. Arsenopyrite is the predominant sulfide and was formed in the first hydrothermal stage. Pyrite and bismuthinite were deposited simultaneously with arsenopyrite. No elevated gold was found as a trace element in arsenopyrite and pyrite, containing only up to 5 ppm Au.

In the second, gold-bearing hydrothermal stage, bismuthinite continued to crystallize and minor amounts of native bismuth, chalcopyrite, tetrahedrite, sphalerite, galena, pyrrhotite and native gold containing up to 10 wt% Ag, were also deposited. Native gold mainly occurs in fine grains up to 20 μm in size, hosted by arsenopyrite and scorodite. This gold is polycrystalline and, if not entirely, at least partly consists of nanocrystals 20–30 nm in size. It often accompanies bismuthinite and native bismuth, filling the cavities and microcracks in arsenopyrite, but mostly where this sulfide has oxidized to scorodite. In that way, these minerals formed an As-Au-Bi assemblage.

The formation of arsenate minerals – scorodite and subsidiary Bi-arsenate, represents the third stage of deposition. These two minerals replacing arsenopyrite and bismuthinite, respectively, represent typical products of sulfide oxidation which were formed either by weathering process or, what we suggest in the case of Dranjak, from a low-temperature solution in a terminal phase of the hydrothermal stage. Anyhow, predominant scorodite is Au-enriched and contain relict gold grains retained after arsenopyrite oxidation (I generation of gold), as well as co-precipitated colloidal-like gold, recognized as the II gold generation.

Declaration of Competing Interest

The authors declare that they have no known competing financial interests or personal relationships that could have appeared to influence the work reported in this paper.

Data availability

Data will be made available on request.

Acknowledgement

We are grateful to two anonymous referees for their helpful comments that improved and clarified the manuscript, as well as to the Associate Editor for careful and constructive handling of the manuscript. We acknowledge the support from ARRS, P1-0417, BI-RS/18-19-035 and 451-03-47/2023-01/200126.

References

Acosta-Góngora, P., Gleeson, S.A., Samson, I.M., Ootes, L., Corriveau, L., 2015. Gold refining by bismuth melts in the iron oxide-dominated NICO Au-Co-Bi (±Cu±W) deposit, NWT, Canada. Economic Geology 110, 291–314. https://doi.org/10.2113/econgeo.110.2.291.

Akiska, S., Ülnü, T., Sayili, I.S., 2008. Mining geology of the gold occurrences related to the arsenopyrites of Izmir-Ödemiş region. Bulletin of the Mineral Research and Exploration 136, 1–16.

Albrecht, M., Derrey, I.T., Horn, I., Schuth, S., Weyer, S., 2014. Quantification of trace element contents in frozen fluid inclusions by UV-fs-LA-ICP-MS analysis. Journal of Analytical Atomic Spectrometry 29, 1034–1041.

Ballantyne, J.M., Moore, J.N., 1988. Arsenic geochemistry in geothermal systems. Geochimica Et Cosmochimica Acta 52, 475–483. https://doi.org/10.1016/0016-7037(88)90102-0.

Bedlivy, D., Mereiter, K., 1982. Preisingerite, Bi3O(OH)(AsO4)2, a new species from San Juan Province, Argentina: its description and crystal structure. American Mineralogist 67, 833–840.

Bindi, L., Moelo, Y., Leone, P., Suchaud, M., 2012. Stoichiometric arsenopyrite, FeAsS, from La Roche-Balue quarry, Loire-Atlantique, France: Crystal structure and mossbauer study. Canadian Mineralogist 50, 471–479.

Boboev, I.R., Tabarov, F.S., 2021. Removal of scorodite arsenic from gold ore in the form of AS2S3 and AS4S4. Hydrometallurgy 199, 105530. https://doi.org/10.1016/j.hydromet.2020.105530.

Bowell, R.J., 1992. Supergene ogld mineralogy at Achanti, Ghana: Implications for the supergene behavior of gold. Mineralogical Magazine 56, 545–560.

Boyle, R.W., Alexander, W.M., Aslin, G.E.M., 1975. Some observations on the solubility of gold. Geological Survey of Canada. Dept. of Energy, Mines and Resources, Paper 75–24, 6 p.

Cabri, L.J., Chryssoulis, S.L., de Villiers, J.P.R., Laflamme, J.H.G., Buseck, P.R., 1989. The nature of "invisible" gold in arsenopyrite. Canadian Mineralogist 27, 353–362.

Cabri, L.J., Newville, M., Gordon, R.A., Crozier, E.D., Sutton, S.R., McMahon, G., Jiang, D.T., 2000. Chemical speciation of gold in arsenopyrite. Canadian Mineralogist 38, 1265–1281. https://doi.org/10.2113/gscanmin.38.5.1265.

Cherepanova, N.V., 2009. Geological and geochemical features of the auriferous Butarny deposit. Moscow University Geology Bulletin 64, 383–385.

Ciobanu, C.L., Birch, W.D., Cook, N.J., Pring, A., Grundler, P.V., 2010. Petrogenetic significance of Au–Bi–Te–S associations: The example of Maldon, Central Victorian gold province, Australia. Lithos 116, 1–17. https://doi.org/10.1016/j.lithos.2009.12.004.

Cook, N.J., Chryssoulis, S., 1990. Concentrations of "invisible gold" in the common sulfides. Canadian Mineralogist 28, 1–16.

Cook, N.J., Ciobanu, C.L., Meria, D., Silcock, D., Wade, B., 2013. Arsenopyrite-pyrite association in an orogenic gold ore: tracing mineralization history from textures and trace elements. Economic Geology 108, 1273–1283.

Craw, D., MacKenzie, D., Grieve, P., 2015. Supergene gold mobility in orogenic gold deposits, Otago Schist, New Zealand. New Zealand Journal of Geology and Geophysics 58 (2), 123–136.

Cvetković, V., Pécskay, Z., Šarić, K., 2013. Cenozoic igneous tectonomagmatic events in the Serbian part of the Balkan peninsula: inferences from K/Ar geochronology. Acta Volcanologica 25, 111–120. https://doi.org/10.1016/j.jv.

Deady, E., Moon, C., Moore, K., Goodenough, K.M., Shail, R.K., 2022. Bismuth: Economic geology and value chains. Ore Geology Reviews 143, 104722. https://doi.org/10.1016/j.oregeorev.2022.104722.

Deleon, G., 1954. A contribution to knowledge of sulfide mineralisations of the western and southern slopes of Željin Mt. Recueil des travaux de l'Institut de géologie "Jovan Žujović" No 7, 105-116.

Douglas, N., Mavrogenes, J., Hack, A., England, R., 2000. The liquid bismuth collector model: An alternative gold deposition mechanism, in: Proceedings of the 15th Understanding Planet Earth, Searching for a Sustainable Future. In: On the Starting Blocks of the Third Millennium: Australian Geological Convention, p. 135.

Dove, P.M., Rimstidt, J.D., 1985. The solubility and stability of scorodite, FeAsO4 x 2H2O. American Mineralogist 70, 838–844.

Einaudi, M.T., Hedenquist, J.W., Inan, E.E. 2003. Sulfidation state of fluids in active and extinct hydrothermal systems: Transitions from porphyry to epithermal environments, in: Volcanic, geothermal, and ore-forming fluids: Rulers and witnesses of processes within the Earth, chapter 15 (S.F. Simmons & I. Graham, eds). Society of Economic Geologist, Special Publication, 10, 285-313.

Fleet, M.E., Chryssoulis, S.L., MacLean, P.J., Davidson, R., Weisener, C.G., 1993. Arsenian pyrite from gold deposits: Au and As distribution investigated by SIMS and EMP, and color staining and surface oxidation by XPS and LIMS. Canadian Mineralogist 31, 1–17.

Fleet M.E., MacLean P.J., Barbier J.,1989. Oscillatory-zoned As-bearing pyrite from strata-bound and stratiform gold deposits: An indicator of ore fluid evolution. In The Geology of Gold Deposits: The Perspectives in 1988, 6 (eds. R.R. Keays, W.R.H. Ramsay, D.I. Groves), 356-362. Economic Geology Monographs.

Fleet, M.E., Mumin, A.H., 1997. Gold-bearing arsenian pyrite and marcasite and arsenopyrite from Carlin Trend gold deposits and laboratory synthesis. American Mineralogist 82, 182–193.

Fougerouse, D., Reddy, S.M., Saxey, D.W., Rickard, W.D.A., van Riessen, A., Micklethwaite, S., 2016. Nanoscale gold clusters in arsenopyrite controlled by growth rate not concentration: Evidence from atom probe microscopy. American Mineralogist 101, 1916–1919. https://doi.org/10.2138/am-2016-5781CCBYNCND.

Frost, R.L., Čejka, J., Sejkora, J., Plášil, J., Reddy, B.J., Keeffe, E.C., 2011. Raman spectroscopic study of a hydroxy-arsenate mineral containing bismuth – atelestite Bi2O(OH)(AsO4). Spectrochimica Acta Part a: Molecular and Biomolecular Spectroscopy 78, 494–496. https://doi.org/10.1016/j.saa.2010.11.016.

Genkin, A.D., Bortnikov, N.S., Cabri, L.J., Wagner, F.E., Stanley, C.J., Safonov, Y.G., McMahon, G., Friedl, J., Kerzin, A.L., Gamyanin, G.N., 1998. A multidisciplinary study of invisible gold in arsenopyrite from four mesothermal gold deposits in Siberia, Russian Federation. Economic Geology 93, 463–487. https://doi.org/10.2113/gsecongeo.93.4.463.

Gomez, M.A., Assaaoudi, H., Becze, L., Cutler, J.N., Demopoulos, G.P., 2010. Vibrational spectroscopy study of hydrothermally produced scorodite (FeAsO4·2H2O), ferric arsenate sub-hydrate (FAsH; FeAsO4·0.75H2O) and basic ferric arsenate sulfate (BFAS; Fe[(AsO4)1–x(SO4)x(OH)x]·wH2O). Journal of Raman Spectroscopy 41, 212–221. https://doi.org/10.1002/jrs.2419.

Guillong, M., Meier, D.L., Allan, M.M., Heinrich, C.A., Yardley, B.W.D., 2008. SILLS: A Matlab-Based Program for the Reduction of Laser Ablation ICP–MS Data of Homogeneous Materials and Inclusions. Mineral. Assoc. Canada Short Course 40, 328–333.

Harvey, M.C., Schreiber, M.E., Rimstidt, J.D., Griffith, M.M., 2006. Scorodite dissolution kinetics: implication for arsenic release. Environmental Science and Technology 40, 6709–6714. https://doi.org/10.1021/es061399f.

Heinrich, C.A., Eadington, P.J., 1986. Thermodynamic predictions of the hydrothermal chemistry of arsenic, and their significance for the paragenetic sequence of some cassiterite-arsenopyrite-base metal sulfide deposits. Economic Geology 81, 511–529. https://doi.org/10.2113/gsecongeo.81.3.511.

Heinrich, C.A., Neubauer, F., 2002. Cu – Au – Pb – Zn – Ag metallogeny of the Alpine – Balkan – Carpathian – Dinaride geodynamic province. Mineralium Deposita 37, 533–540.

Hinchey, J.G., Wilton, D.H.C., Tubrett, M.N., 2003. A LAM-ICP-MS study of the distribution of gold in arsenopyrite from the Lodestar prospect, Newfoundland, Canada. Canadian Mineralogist 41, 353–364. https://doi.org/10.2113/gscanmin.41.2.353.

Horn, I., 2008. Comparison of femtosecond and nanosecond interactions with geologic matrices and their influence on accuracy and precision of LA-ICP-MS data. Mineral. Assoc. Canada Short Course 40, 53–65.

Hough, R.M., Noble, R.R.P., Reich, M., 2011. Natural gold nanoparticles. Ore Geology Reviews 42, 55–61. https://doi.org/10.1016/j.oregeorev.2011.07.003.

Ishbobaev, T., Tangirov, A., Khalilov, A., Muratova, M., 2021. Some features of the formation of the oxidation zone of the Kokpatas ore field in Uzbekistan. IOP Conf. Series: Earth and Environmental Science 937, 042083. IOP Publishing doi:10.1088/1755-1315/937/4/042083.

Janković, S., 1997. The Carpatho-Balkanides and adjacent area: a sector of the Tethyan Eurasian metallogenic belt. Mineralium Deposita 32, 426–433.

Jonasson, D., 2018. Mobilization and occurrence of gold within arsenopyrite veins Akçaabat deposit, southwestern Turkey. Department of Earth Sciences, University of Gothenburg (Sweden), p. 33 pp.. Master thesis,.

Jones, R.A., Nesbitt, H.W., 2002. XPS evidence for Fe and As oxidation states and electronic states in loellingite (FeAs2). American Mineralogist 87, 1692–1698.

Kalinin, Y.A., Kovalev, K.R., Naumov, E.A., Kirillov, M.V., 2009. Gold in the weathering crust at the Suzdal' deposit (Kazakhstan). Russian Geology and Geophysics 50, 174–187. https://doi.org/10.1016/j.rgg.2008.09.002.

Krause, E., Ettel, V.A., 1988. Solubility and stability of scorodite, FeAsO4 x 2H2O: New data and further discussion. American Mineralogist 73, 850–854.

Lesić, V., Márton, E., Cvetkov, V., Tomić, D., 2013. Magnetic anisotropy of Cenozoic igneous rocks from the Vardar zone (Kopaonik area, Serbia). Geophysical Journal International 193, 1182–1197.

Lesić, V., Márton, E., Gajić, V., Jovanović, D., Cvetkov, V., 2019. Clockwise vertical-axis rotation in the West Vardar zone of Serbia: tectonic implications. Swiss Journal of Geosciences 112, 199–215. https://doi.org/10.1007/s00015-018-0321-8.

Madox, L.M., Bancroft, G.M., Scaini, M.J., Lorimer, J.W., 1998. Invisible gold: Comparison of Au deposition on pyrite and arsenopyrite. America Mineralogist 83, 1240–1245.

Majzlan, J., Drahota, P., Filippi, M., Grevel, K., Kahl, W., Plasil, J., Boerio-Goates, J., Woodfield, B.F., 2012. Thermodynamic properties of scorodite and parascorodite (FeAsO4•2H2O), kankite (FeAsO4•3.5H2O), and FeAsO4. Hydrometallurgy 117–118, 47–56.

Maksimović, Z., Divljan, S., 1953. The results of geological-petrographic mapping and observation of ore occurrences in the areas of Plana and Gokčanica on the western slopes of Željin. Book of abstracts S.A.N. XXXIII-Geological Institute s.a.n. Book 5, 223–253. In Serbian.

Meng, L., Huang, F., Gao, W., Gao, R., Zhao, F., Zhou, Y., Li, Y., 2022. Multi-step gold refinement and collection using Bi-minerals in the Laozuoshan gold deposit. NE China. Minerals 12, 1137. https://doi.org/10.3390/min12091137.

Möller, P., Kersten, G., 1994. Electrochemical accumulation of visible gold on pyrite and arsenopyrite surfaces. Mineralium Deposita 29, 404–413.

Möller, P., Sastri, C.S., Kluckner, M., Rhede, D., Ortner, H.M., 1997. Evidence for electrochemical deposition of gold onto arsenopyrite. European Journal of Mineralogy 9, 1217–1226.

Mumin, A.H., Fleet, M.E., Chryssoulis, S.L., 1994. Gold mineralization in As-rich mesothermal gold ores of the Bogosu-Prestea mining district of the Ashanti Gold Belt, Ghana: Remobilization of "invisible" gold. Mineralium Deposita 29, 445–460.

Murciego, A., Alvarez-Ayso, E., Pellitero, E., Rodríguez, M.A., Sánchez, A.G., Tamayo, A., Rubio, J., Rubio, F., Rubín, J., 2011. Study of arsenopyrite weathering products in mine wastes from abandoned tungsten and tin exploitations. Journal of Hazardous Materials 186, 590–601.

Oeser, M., Weyer, S., Horn, I., Schuth, S., 2014. High-precision Fe and Mg isotope ratios of silicate reference glasses determined in situ by femtosecond LA-MC-ICP-MS and by solution nebulisation MC-ICP-MS. Geostandards and Geoanalytical Research 38, 311–328. https://doi.org/10.1111/j.1751-908X.2014.00288.x.

Pačevski, A., 2002. Mineralogical-crystallographic and paragenetic characteristics of arsenopyrite from the Gokčanica area (Željin Mt.). In: Serbian. Faculty of Mining and Geology, University of Belgrade (Serbia), p. 40 pp.. Diploma thesis,.

Palenik, C.S., Utsunomiya, S., Reich, M., Kesler, S.E., Wang, L., Ewing, R.C., 2004. "Invisible" gold revealed: Direct imaging of gold nanoparticles in a Carlin-type deposit. American Mineralogist 89, 1359–1366. https://doi.org/10.2138/am-2004-1002.

Pokrovski, G.S., Gout, R., Schott, J., Zotov, A., Harrichoury, J.C., 1996. Thermodynamic properties and stoichiometry of the As (III) hydroxide complexes at hydrothermal conditions. Geochimica Et Cosmochimica Acta 60, 737–749. https://doi.org/10.1016/0016-7037(95)00427-0.

Pokrovski, G.S., Kara, S., Roux, J., 2002. Stability and solibility of arsenopyrite, FeAsS, in crustal fluids. Geochimica Et Cosmochimica Acta 66, 2361–2378. https://doi.org/10.1016/S0016-7037(02)00836-0.

Pokrovski, G.S., Escoda, C., Blanchard, M., Testemale, D., Hazemann, J.L., Gouy, S., Kokh, M.A., Boiron, M.C., de Parseval, F., Aigouy, T., Menjot, L., de Parseval, P., Proux, O., Rovezzi, M., Béziat, D., Salvi, S., Kouzmanov, K., Bartsch, T., Pöttgen, R., Doert, T., 2021. An arsenic-driven pump for invisible gold in hydrothermal systems. Geochemical Perspectives Letters 17, 39–44.

Popović, R., 1992. The occurrence of precious metals in Međurečje (valley of the Gokčanica river) near Ušće. Ann. Géol. Penins. Balk 56, 383–398. In Serbian.

Reich, M., Kesler, S.E., Utsunomiya, S., Palenik, C.S., Chryssoulis, S.L., Ewing, R.C., 2005. Solubility of gold in arsenian pyrite. Geochimica Et Cosmochimica Acta 69, 2781–2796. https://doi.org/10.1016/j.gca.2005.01.011.

Roussel, C., Néel, C., Bril, H., 2000. Minerals controlling arsenic and lead solubility in an abandoned gold mine tailings. Science of the Total Environment 263, 209–219. https://doi.org/10.1016/S0048-9697(00)00707-5.

Salzsaueler, K.A., Sidenko, N.V., Sherriff, B.L., 2005. Arsenic mobility in alteration products of sulfide-rich arsenopyrite-bearing mine wastes, Snow Lake, Manitoba, Canada. Applied Geochemistry 20, 2303–2314.

Saunders, J.A., 1990. Colloidal transport of gold and silica in epithermal precious-metal systems: Evidence from the Sleeper deposit, Nevada. Geology 18, 757–760.

Sejkora, J., Ondruš, P., Fikar, M., Veselovský, F., Mach, Z., Gabašová, A., Škoda, R., Beran, P., 2006. Supergene mineral at the Huber stock and Schnöd stock deposits, Krásno ore district, the Slavkovský les area, Czech Republic. Jorunal of the Czech Geological Society 51, 57–101. https://doi.org/10.3190/JCGS.989.

Shibata, E., Onodera, N., Fujita, T., Nakamura, T., 2012. Elusion tests of scorodite synthesized by oxidation of ferrous ions. Resources Processing 59, 42–48.

Singhania, S., Wang, Q., Filippou, D., Demopoulos, G.P., 2005. Temperature and seeding effects on the precipitation of scorodite from sulfate solutions under atmospheric-pressure conditions. Metallurgical and Materials Transactions B 36, 327–333.

Stoffregen, R., 1986. Observations on the behavior of gold during supergene oxidation at Summitville, Colorado, U.S.A., and implications for electrum stability in the weathering environment. Applied Geochemistry 1, 549–558.

Stokes, H.N., 1906. Experiments on the solution, transportation, and deposition of copper, silver, and gold. Economic Geology 1, 644–650.

Sung, Y.H., Brugger, J., Ciobanu, C.L., Pring, A., Skinner, W., Nugus, M., 2009. Invisible gold in arsenian pyrite and arsenopyrite from a multistage Archaean gold deposit: Sunrise Dam, Eastern Goldfields Province, Western Australia. Mineralium Deposita 44, 765–791.

Tooth, B., Brugger, J., Ciobanu, C., Liu, W., 2008. Modeling of gold scavenging by bismuth melts coexisting with hydrothermal fluids. Geology 36, 815–818. https://doi.org/10.1130/G25093A.1.

Urosević, M., Pavlović, Z., Klisić, M., Brković, T., Mališević, M., Stefanović, M., Marković, O., Trifunović, S., 1973a. Geological map and explanatory notes of the Basic Geological Map of SFRJ, sheet Vrnjci (1:100 000), Savezni Geoloski Zavod, Beograd, 69 pp. In Serbian.

Urosević, M, Pavlović, Z., Klisić, M. et al., 1973b. Geological Map and Explanatory Notes of the Basic Geological Map of SFRJ, sheet Novi Pazar (1:100 000), Savezni Geoloski Zavod, Beograd, 77 pp. In Serbian.

Vranić, M., 2021. The impact of Medieval Mining upon the environment of the Central Balkans. Issues in Ethnology and Anthropology, 16, 723-738. In Serbian; abstract in English and French. 10.21301/eap.v16i3.5.

Walker, S.R., Parsons, M.B., Jamieson, H.E., Lanzirotti, A., 2009. Arsenic mineralogy of near-surface tailings and soils: Influences on arsenic mobility and bioaccessibility in the Nova Scotia Gold mining districts. Canadian Mineralogist 47, 533–556. https://doi.org/10.3749/canmin.47.3.533.

Xu, Y., Zhou, G.P., Zheng, X.F., 2007. Redetermination of iron(III) arsenate dehydrate. Acta Crystallographica Section E 63, i67–i69. https://doi.org/10.1107/S1600536807005302.

Zelić, M., Levi, N., Malasoma, A., Marroni, M., Pandolfi, L., Trivić, B., 2010. Alpine tectono-metamorphic history of the continental units from Vardar Zone: the Kopaonik metamorphic complex (Dinaric-Hellenic belt, Serbia). Geological Journal 45, 59–77.